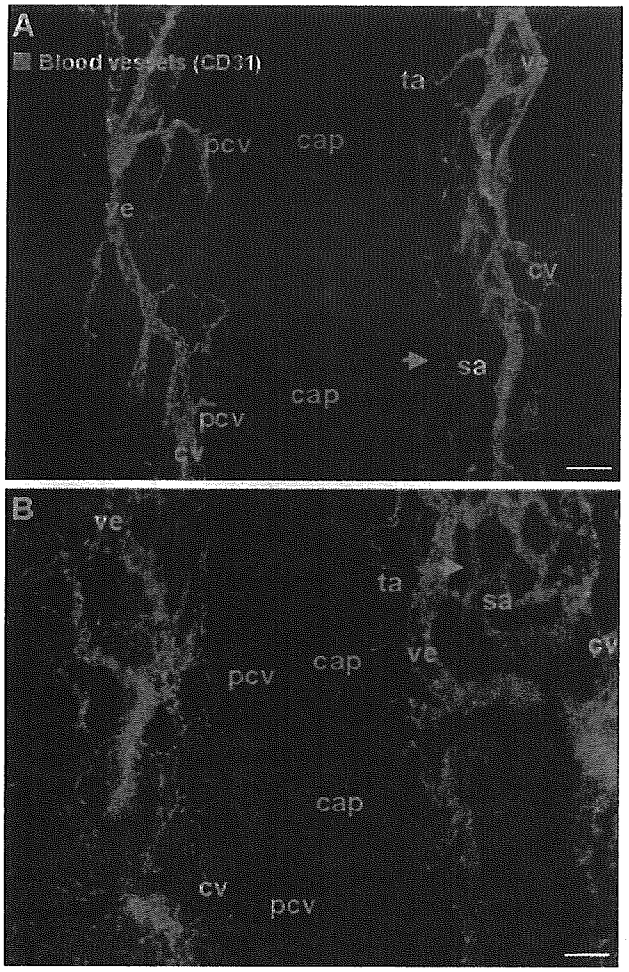

Figure 1. Effect of systemic COMP-Ang1 protein treatment on blood vessels in mouse tracheal mucosa. FVB/N mice were treated with daily injections of 200 μg of BSA (A) or 200 μg of COMP-Ang1 recombinant protein (B) for 14 days. Blood vessels in tracheal whole mounts were visualized with PECAM-1 (CD31) immunostaining (red). Six segments of the microvascular hierarchy are evident: segmental arteriole (sa, arrows), terminal arteriole (ta), capillary (cap), postcapillary venule (pcv), collecting venule (cv), and venule (ve). Of these, postcapillary venules and the venous ends of capillaries were the most enlarged after treatment by COMP-Ang1. The results from 4 experiments were similar. Scale bar=50 μm.

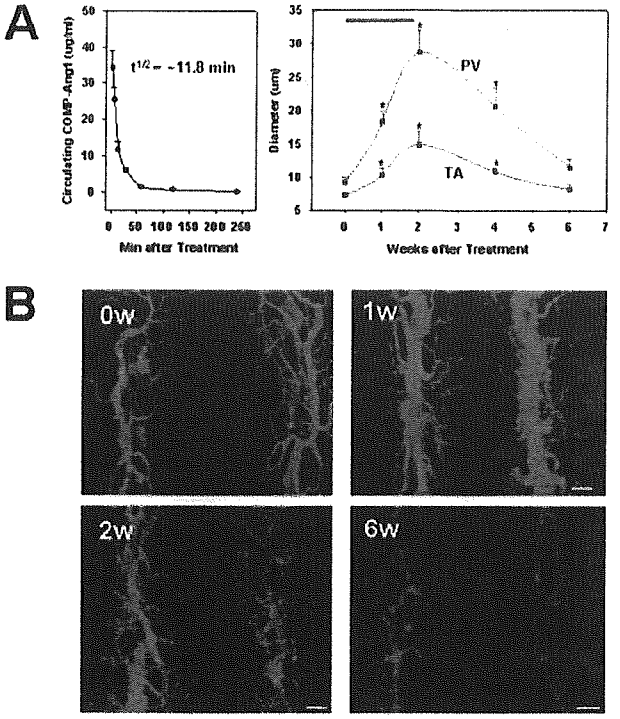

Figure 2. Effect of systemic COMP-Ang1 protein treatment on postcapillary venules and terminal arterioles. FVB/N mice were treated by daily injection of COMP-Ang1 recombinant protein (200 μg) for 14 days (A, black bar). At the indicated times, tracheal vessels were visualized with PECAM-1 immunostaining (B, red). The diameter of postcapillary venules and terminal arterioles are shown (A, right). Circulating plasma levels of COMP-Ang1 were measured by ELISA after a single injection of COMP-Ang1 recombinant protein (200 μg/mouse) (A, left). Diameters of 35 to 40 postcapillary venules (PV)/5 fields (brown curve) and 10 to 12 terminal arterioles (TA)/10 fields (blue curve) were measured at the edge of cartilage rings in each mouse. Values are mean±SD from 4 to 5 mice. *$P<0.05$ vs control period. COMP-Ang1 induced enlargement of postcapillary venules, collecting venules, venous ends of capillaries, venules, and terminal arterioles for up to 2 weeks, and then the enlarged blood vessels returned gradually to normal after discontinuation of the COMP-Ang1 treatment. Scale bar=50 μm.

of tracheal vessels, again in a reversible manner (data not shown). In comparison, the diameters of tracheal vessels were indistinguishable between the control and experimental periods in tracheal vessels of mice treated with BSA (data not shown). These results indicate that short-term spikes of circulating COMP-Ang1 induce reversible enlargement of some tracheal vessels.

Long-Term and Sustained Circulating COMP-Ang1 Induces Long-Lasting Enlargement of Postcapillary Venules and Terminal Arterioles in Tracheal Vessels

As an alternative method for systemic treatment with COMP-Ang1, an adenoviral vector encoding the COMP-Ang1 gene (Ade-COMP-Ang1) was developed. As a control, an adenoviral vector encoding the LacZ gene (Ade-LacZ) was developed. The potency, solubility, oligomerization status, and stability of the COMP-Ang1 produced from HEK293 cells transduced with Ade-COMP-Ang1 are similar to that of COMP-Ang1 produced from COS-7 cells transiently transfected with plasmid vector containing the COMP-Ang1 gene[10] (data not shown). Adult mice were treated with 1×10^9 pfu Ade-COMP-Ang1 or Ade-LacZ. At multiple times more than a period of 16 weeks, circulating plasma COMP-Ang1 levels were measured, and blood vessels in tracheal mucosa were visualized with PECAM-1 immunostaining (Figure 3). Circulating COMP-Ang1 increased as early as 12 hours after treatment, peaked at 1 to 2 weeks, declined gradually thereafter, and returned to control levels at 6 weeks after treatment (Figure 3A). The peak concentrations of circulating COMP-Ang1 were ≈3.5 to 4.5 μg. Significant enlargement of postcapillary venules, capillaries (distinctively, only the venous end of capillaries was enlarged), collecting venules, and terminal arterioles, but not segmental arterioles, was notice-

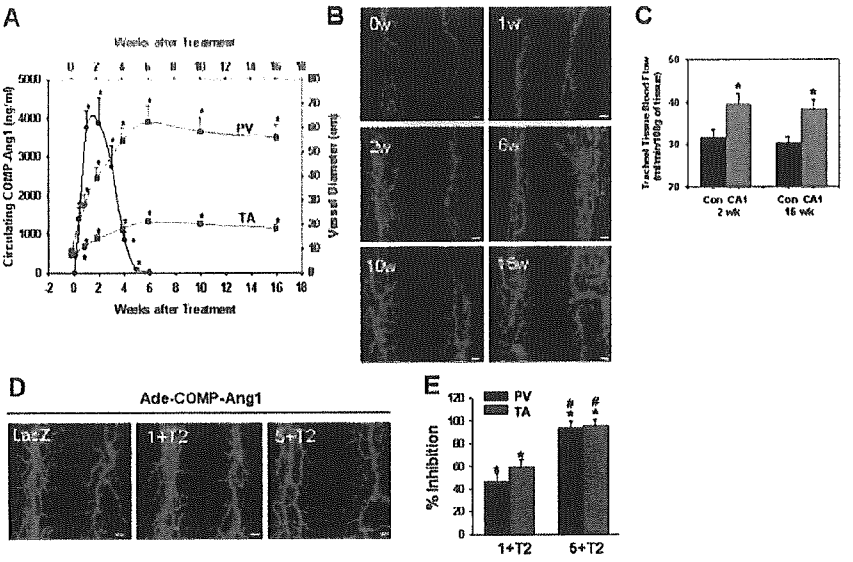

Figure 3. Effect of adenoviral COMP-Ang1 on postcapillary venules and terminal arterioles and blood flow. A through D, FVB/N mice were treated with 1×10^9 pfu Ade-COMP-Ang1 (n=6). At the indicated times, circulating plasma levels of COMP-Ang1 were measured by ELISA (A, black circle), and tracheal vessels were visualized with PECAM-1 immunostaining (B, red). The diameters of postcapillary venules (PV, brown curve) and terminal arterioles (TA, blue curve) are shown. Diameters of 35 to 40 PV/5 fields and 10 to 12 TA/10 fields were measured at the edge of cartilage rings in each mouse. Values are mean±SD from 4 to 5 mice. *$P<0.05$ vs control period. Scale bar=50 μm. C, Laser-Doppler flowmetric analyses for tracheal tissue blood flows of the mice treated with 1×10^9 pfu Ade-LacZ (Con) or 1×10^9 pfu Ade-COMP-Ang1 (CA1). Quantification of tracheal blood flows at 2 and 16 weeks after treatment with Con or CA1. Bars represent mean±SD from 4 to 5 mice. *$P<0.05$ vs Con. D and E, FVB/N mice were pretreated with 1×10^8 (1+T2) or 5×10^8 (5+T2) pfu Ade-sTie2-Fc (n=5 each), or 5×10^8 pfu Ade-LacZ (LacZ, n=5) at 24 hours before 1×10^8 pfu Ade-COMP-Ang1 treatment. Two weeks later, tracheal vessels were visualized by PECAM-1 immunostaining (D, red). Scale bar=50 μm. Diameters of 35 to 40 PV/5 fields and 10 to 12 TA/10 fields were measured at the edge of cartilage rings in each mouse. E, Bars represent the mean±SD from 5 experiments as percentage of inhibition of vascular remodeling induced by the pretreatment. Vascular remodeling induced by pretreatment of the Ade-LacZ is arbitrarily given as 100%. *$P<0.05$ vs LacZ, #$P<0.05$ vs 1+T2.

able at 1 week after the Ade-COMP-Ang1 treatment (Figure 3B). The vascular enlargements induced by Ade-COMP-Ang1 increased further for up to 6 weeks and then reached a plateau (Figure 3A and 3B). For example, the diameter of postcapillary venules increased 4.3-fold at 2 weeks, 6.0-fold at 4 weeks, and 6.8-fold at 6 weeks (Figure 3A). The enlargement of terminal arterioles was also significant beginning at 1 week after the treatment and increased in a time-dependent manner. However, the increase in diameter in terminal arterioles was less than that in postcapillary venules (Figure 3A and 3B). Importantly, the size of Ade-COMP-Ang1–induced enlarged blood vessels did not significantly decrease for as long as 16 weeks after the treatment, although circulating COMP-Ang1 returned to the control level at 6 weeks after treatment (Figure 3A). In comparison, diameters of tracheal vessels in mice treated with Ade-LacZ were indistinguishable between the control and experimental periods (data not shown). Using a laser-Doppler flowmeter, tracheal tissue blood flows were measured at 2 weeks (the peak level of circulating COMP-Ang1) and 16 weeks (undetectable level of circulating COMP-Ang1) after Ade-LacZ or Ade-COMP-Ang1 treatment. At 2 weeks, tracheal tissue blood flow was increased ≈25% in the mice treated with Ade-COMP-Ang1 compared with the mice treated with Ade-LacZ (Figure 3C and 3D). At 16 weeks, importantly, increased tracheal tissue blood flow by Ade-COMP-Ang1 was not significantly changed (Figure 3C and 3D). These results indicate that long term and sustained circulating COMP-Ang1 treatment induces long-lasting enlargement of tracheal blood vessels with long-lasting enhancement of tissue blood flow in the adult mice.

Tie2 Activation Is Involved in COMP-Ang1–Induced Vascular Remodeling

To determine the involvement of Tie2 activation in COMP-Ang1–induced vascular remodeling, the mice were pretreated with 1×10^8 pfu or 5×10^8 pfu Ade-sTie2-Fc at 24 hours before 1×10^8 pfu Ade-COMP-Ang1 treatment. Two weeks later, the diameters of postcapillary venules and terminal arterioles were measured. Pretreatment with 1×10^8 pfu or 5×10^8 pfu Ade-sTie2-Fc suppressed COMP-Ang1–induced vascular remodeling to the following extent: 46.5±7.7% or 93.5±6.4% in postcapillary venules and 59.7±6.6% or 95.1±5.7% in terminal arterioles, respectively (Figure 3E and 3F). These data indicate that COMP-Ang1–induced vascular remodeling is mainly mediated through Tie2 activation in adult tracheal vessels.

Long-Term and Sustained Circulating COMP-Ang1 Induces Various Vascular Remodeling in Different Organ

Both mice treated with Ade-LacZ (1×10^9 pfu) and those treated with Ade-COMP-Ang1 (1×10^9 pfu) appeared generally healthy, as they gained weight normally. However, the skin of mice treated with Ade-COMP-Ang1 appeared strikingly redder than the skin of mice treated with Ade-LacZ, beginning 10 to 14 days after the treatment. The Ade-COMP-

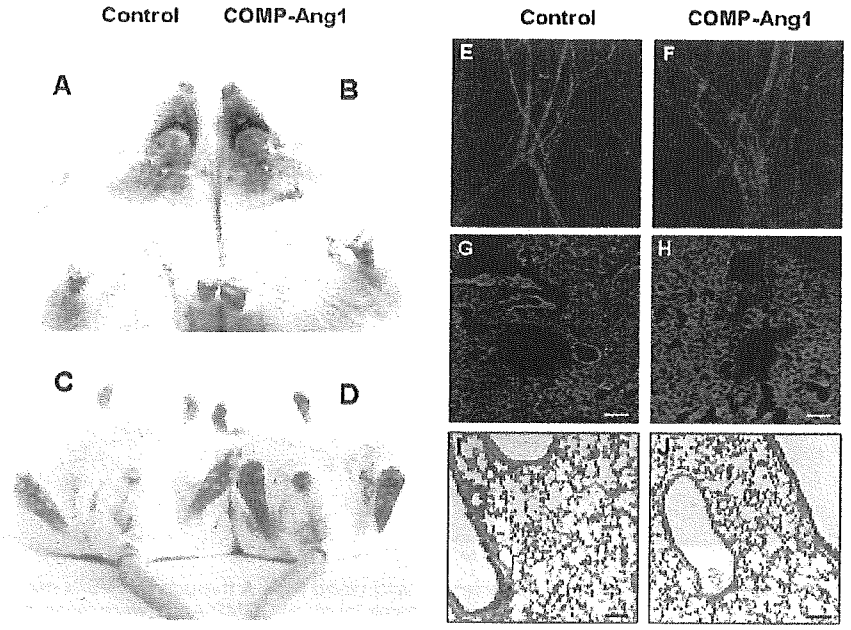

Figure 4. Effect of adenoviral COMP-Ang1 on skin color and vascular remodeling in ear skin and lung at 16 weeks after treatment. FVB/n mice were treated with 1×10^9 pfu Ade-LacZ or Ade-COMP-Ang1. Sixteen weeks later, the skin color of the face, hands, soles, penis, and tail were photographed (A, B, C, and B), blood vessels in ear skin (E and F) and lungs (G and H) were visualized with PECAM-1 (CD31) immunostaining (red), and sections of lungs were stained with H&E (I and J). The mice treated with Ade-COMP-Ang1 show overt skin redness, have prominently enlarged blood vessels in the ear skin, and have more dense PECAM-1–positive endothelial cells in the lung without overt histologic alteration compared with the mice treated with Ade-LacZ. The results from 4 experiments were similar. Scale bar=50 μm.

Ang1–induced skin redness persisted for as long as 16 weeks after the treatment (Figure 4). Sixteen weeks after the treatment, skin color in hair-sparse portions such as the face, hands, soles, penis, and tail of mice treated with Ade-COMP-Ang1 were distinctly redder than those of mice treated with Ade-LacZ. Blood vessels of the ear and capillaries of the heart, adrenal cortex, and liver of the mice treated with Ade-COMP-Ang1 were enlarged (Figures 4 and 5). More PECAM-1–positive endothelial cells were present in the lung, heart, liver, and renal medulla of mice treated with Ade-COMP-Ang1 compared with the mice treated with Ade-LacZ (Figures 4 and 5 and online Figure I in the data supplement). However, blood vessels of the renal cortex, including glomeruli, and intestinal villi of the mice treated with Ade-COMP-Ang1 and the mice treated with Ade-LacZ were indistinguishable. In addition, the body weights, systemic blood pressures, and heart rates of the 2 groups of mice were indistinguishable. These results indicate that long-term and sustained circulating COMP-Ang1 treatment induces long-lasting tissue-specific vascular remodeling in different blood vessels without notable changes in systemic blood pressure and heart rate (online Table I).

Induction of Tie2 Could Be Involved in Permanent Changes of COMP-Ang1–Induced Vascular Remodeling

Based on these observations, we asked whether Tie2 expression was more abundant in postcapillary venules than termi-

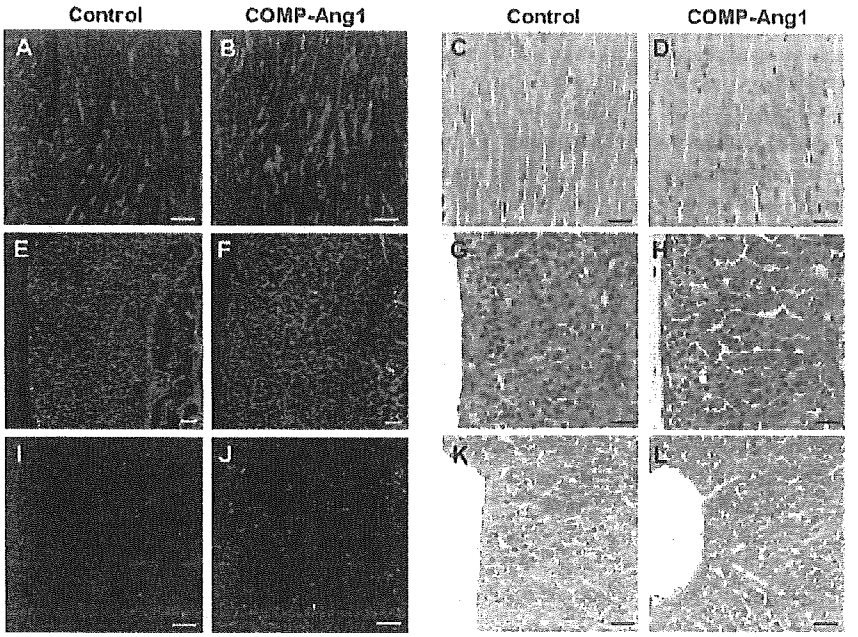

Figure 5. Effect of adenoviral COMP-Ang1 on vascular remodeling in heart, adrenal cortex, and liver at 16 weeks after the treatment. FVB/n mice were treated with 1×10^9 pfu Ade-LacZ or Ade-COMP-Ang1. Sixteen weeks later, blood vessels in heart (A through D), adrenal cortex (E through H), and liver (I through L) were visualized with PECAM-1 (CD31) immunostaining (red), and the sections were stained with H&E. The mice treated with Ade-COMP-Ang1 have enlarged capillaries in the heart and adrenal cortex and more PECAM-1–positive endothelial cells in the liver compared with the mice treated with Ade-LacZ. The results from 4 experiments were similar. Scale bar=25 μm.

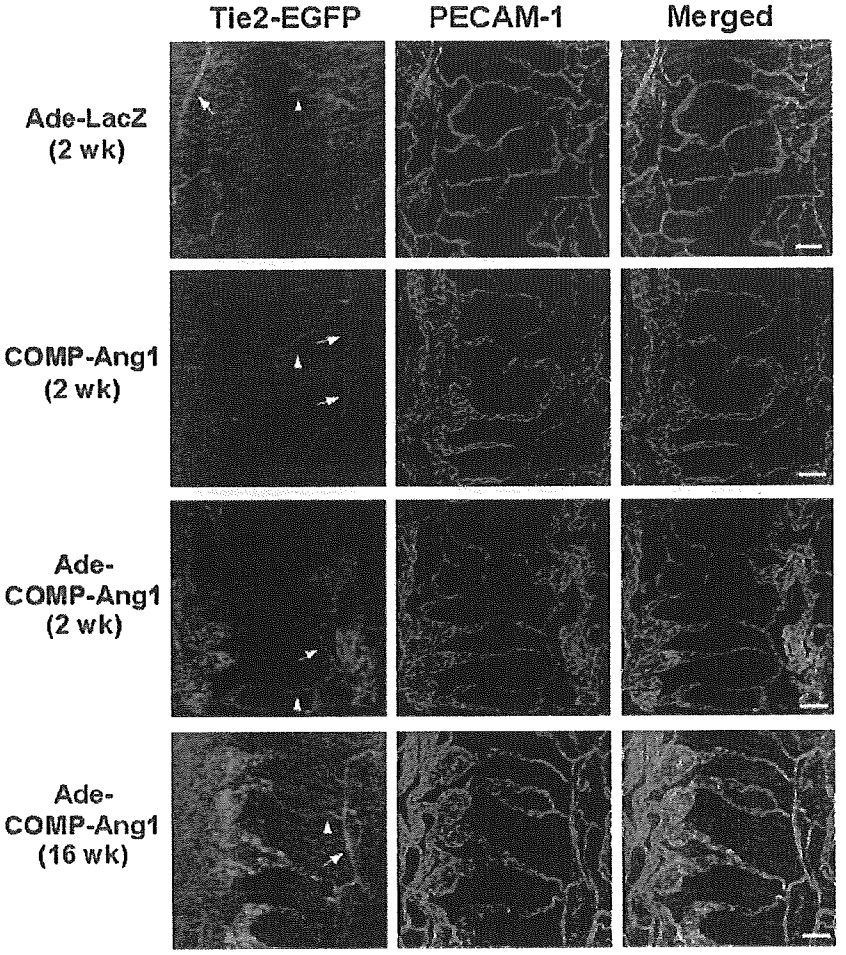

Figure 6. Induction of Tie2 expression in COMP-Ang1–induced vascular remodeling. Tie2-GFP transgenic mice (10 weeks old) were treated with daily injection of 200 μg of COMP-Ang1 recombinant protein (COMP-Ang1) for 2 weeks or a single injection of 1×10^9 pfu Ade-LacZ or Ade-COMP-Ang1. At 2 and 16 weeks after the beginning of the treatments, Tie2 expression in tracheal vessels was visualized by GFP expression (green) and PECAM-1 immunostaining (red), and the images were merged. The results from 4 experiments were similar. Arrowhead indicates terminal arterioles; arrow, precapillary arterioles. Scale bar=50 μm.

nal arterioles in mouse trachea. Therefore, we examined the extent of Tie2 expression using transgenic mice with Tie2 promoter–driven green fluorescent protein (GFP).[12] In the tracheal mucosa of adult mice, Tie2 expression was not detectable in most endothelial cells of postcapillary venules, whereas it was moderately expressed in endothelial cells of terminal and precapillary arterioles of tracheal vessels (Figure 6). Thus, differential enlargement of tracheal vessels on COMP-Ang1 stimulation is not dependent on the extent of Tie2 expression. However, Tie2 expression was markedly increased in endothelial cells of collecting venules, venules, postcapillary venules, and capillaries at 2 weeks after the Ade-COMP-Ang1 treatment (Figure 6), which is somewhat consistent with a recent report with Ade-Ang1.[8] Tie2 expression was further increased in endothelial cells of the same vessels at 16 weeks after the Ade-COMP-Ang1 treatment (Figure 6). In contrast, Tie2 expression was not changed in any endothelial cells of enlarged tracheal vessels at 2 weeks after the recombinant COMP-Ang1 protein treatment (Figure 6). Area densities of Tie2 expression in a given microscopic field area (0.22 mm^2) for arterioles, capillaries, and venules in tracheal mucosa were 8.2±1.7, 2.8±0.4, and 3.3±0.6% (mean±SD from 4 mice), respectively, after Ade-LacZ treatment (at 2 weeks); 7.6±1.9, 3.1±0.5, and 3.7±0.6% after COMP-Ang1 protein treatment (at 2 weeks); 11.3±2.2, 10.3±1.7, and 28.1±5.4% after Ade-COMP treatment (at 2 weeks); and 13.3±2.7, 18.2±3.5, and 47.7±7.2 after Ade-COMP treatment (at 16 weeks). In addition, Tie2 expression was notably higher in the enlarged veins of abdominal skin and the sinusoidal capillaries in liver of the mice treated with Ade-COMP-Ang1 than the mice treated with Ade-LacZ at 16 weeks after the treatment (online Figure II). Thus, Tie2 expression in venular and capillary endothelial cells could be induced with long-term and sustained Tie2 stimulation induced by Ade-COMP-Ang1 but not with short-term spiked Tie2 stimulation induced by recombinant COMP-Ang1 protein.

COMP-Ang1–Induced Vascular Enlargement Could Result From Circumferential Endothelial Cell Proliferation

COMP-Ang1–induced enlargement of blood venules appears to result from endothelial cell proliferation rather than vasodilation or endothelial cell hypertrophy because the endothelial cells were normal in size (Figure 7A and 7B). To test this possibility, we examined by immunostaining the number of endothelial cells positive for phosphohistone H3 (nuclear protein of diving cell). Numerous phosphohistone H3–positive immunostained endothelial cells were detected in various portions including postcapillary venules, capillaries, collect-

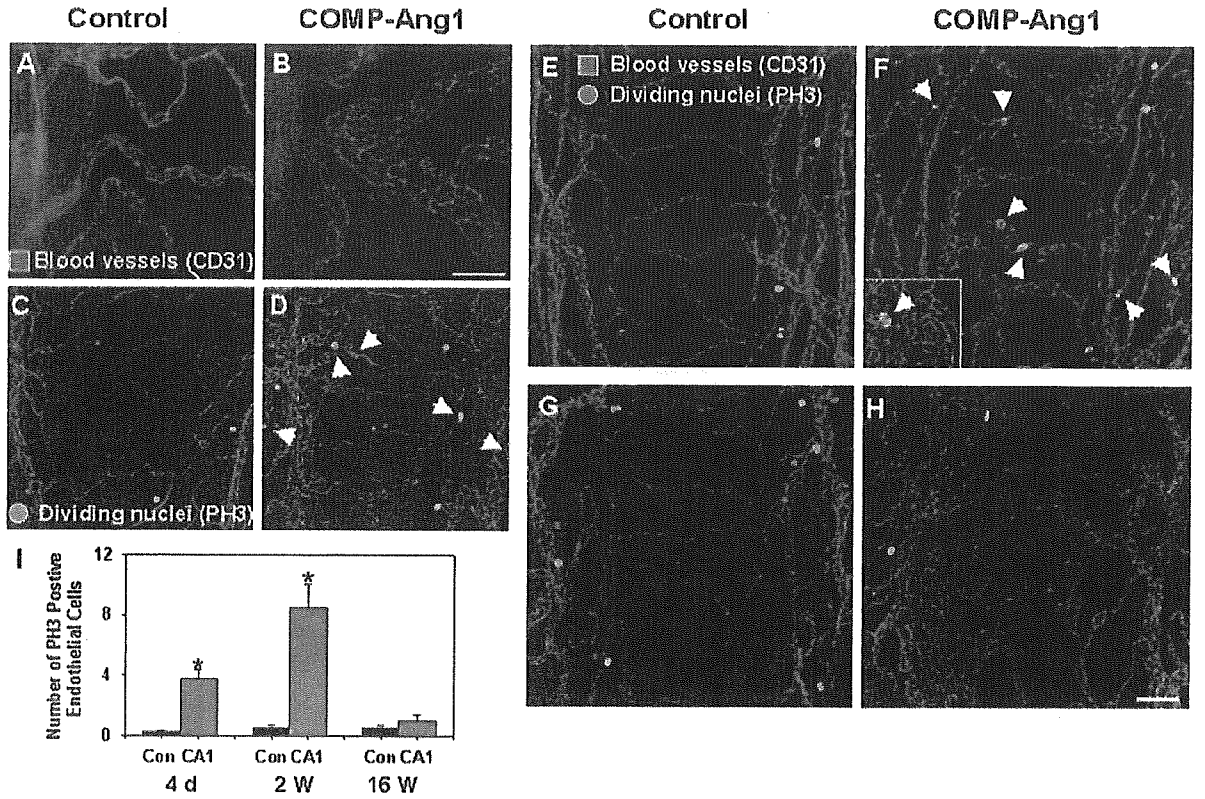

Figure 7. Increased number of dividing endothelial cells during COMP-Ang1–induced enlargement. FVB/N mice were treated with 1×10^9 pfu Ade-LacZ (control; A, C, E, and G) or Ade-COMP-Ang1 (COMP-Ang1; B, D, F, and H). Four days (C and D), 2 weeks (E and F), and 16 weeks (G and H) later, tracheal vessels were visualized with PECAM-1 (CD31) immunostaining (red) and phosphohistone H3 (PH3) immunostaining (green). F, Arrow indicates PH3-immunopositive endothelial cells; white square, PH3-immunopositive endothelial cells in postcapillary venule at higher magnification. Scale bar=50 μm. I, Number of PH3-immunopositive endothelial cells in a given 0.21 mm^2 area. Bars represent mean±SD from 4 mice. Con indicates control; CA1, COMP-Ang1. *$P<0.05$ vs Con.

ing venules, venules, and terminal arterioles of tracheal vessels at 4 days and 2 weeks after the Ade-COMP-Ang1 treatment (Figure 7D, 7F, and 7I) or after recombinant COMP-Ang1 protein treatment (data not shown). However, almost no phosphohistone H3–positive endothelial cells were detected in any portion of tracheal vessels at 4 days or 2 and 16 weeks after the Ade-LacZ treatment and at 16 weeks after the Ade-COMP-Ang1 treatment (Figure 7C, 7E, 7G, and 7I). These findings indicate that vascular enlargement induced by COMP-Ang1 is more likely to result from endothelial cell proliferation depending on concentration of circulating COMP-Ang1 than from vasodilation or endothelial cell hypertrophy.

COMP-Ang1–Induced Postcapillary Venule Enlargement Is Not Accompanied by Pericyte Recruitment

Ang1 is known to be a strong growth factor for pericyte recruitment to nascent endothelial cells during vasculogenesis in physiological and pathological conditions.[3–5] Therefore, we examined the interaction between endothelial cells and pericytes in the enlarged blood vessels of the trachea by double-immunostaining for endothelial cells and pericytes at 4 weeks after Ade-LacZ or Ade-COMP-Ang1 treatment. The interaction of endothelial cells and pericytes in most of tracheal blood vessels (except postcapillary venules) in mice that received Ade-COMP-Ang1 was similar to that in mice that received Ade-LacZ (Figure 8). Although less interaction of endothelial cells with pericytes was found on the enlarged postcapillary venules than elsewhere, the number of pericytes of the enlarged postcapillary venules was similar to the control postcapillary venules (Figure 8). Thus, COMP-Ang1 did not promote pericyte recruitment to the COMP-Ang1–induced enlarged venules in the trachea.

Discussion

The most important and novel finding in this study is that enlargement of tracheal blood vessels and enhancement of tracheal tissue blood flow induced by long-term and sustained exposure to COMP-Ang1 had not regressed for up to 16 weeks, despite the fact that exposure to COMP-Ang1 had already been discontinued at 6 to 7 weeks in adult mice. In comparison, enlargement of tracheal blood vessels induced by short-term intermittent exposure to COMP-Ang1 regressed on discontinuation of recombinant COMP-Ang1 treatment. Therefore, long-lasting vascular enlargement and enhancement of blood flow can be achieved by long-term and sustained exposure to COMP-Ang1.

Like other therapeutic proteins, circulating COMP-Ang1 rapidly disappeared in the plasma, probably because of its trapping by the Tie2 receptor of lung endothelial cells.[15]

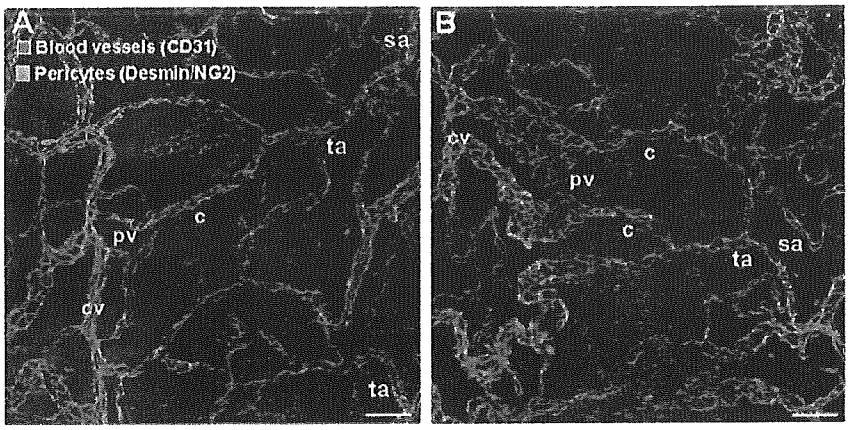

Figure 8. Interaction between endothelial cells and pericytes in COMP-Ang1–induced enlarged tracheal vessels. FVB/n mice were treated with 1×10^9 pfu Ade-COMP-Ang1 (B) or Ade-LacZ (A). Four weeks later, tracheal vessels were visualized with PECAM-1 (CD31) immunostaining (red), and pericytes were visualized with desmin/NG2 immunostaining (green). The results from 4 experiments were similar. Scale bar=50 μm.

However, we were able to achieve long-term (>4 weeks) and sustained (>1000 ng/mL) circulating COMP-Ang1 in mice by a single intravenous injection of 1×10^9 pfu Ade-COMP-Ang1. Throughout these experiments, we learned that long-term (≈6 weeks) and sustained exposure to COMP-Ang1 produced long-lasting enlargement of postcapillary venules and terminal arterioles in the tracheal mucosa, whereas short-term (≈2 weeks) and intermittent exposure to COMP-Ang1 produced reversible enlargements of these vessels. Similar to our results, another study found that long-term (4 weeks) sustained exposure to vascular endothelial growth factor (VEGF) produced long-lasting acquired vascular remodeling in liver, whereas short-term (2 weeks) sustained exposure to VEGF produced reversible vascular remodeling.[16] What are the major mechanisms and factors that produce long-lasting and reversible vascular remodeling? Is there a threshold stimulation of Tie2 by COMP-Ang1 that can produce permanent enlargement? Our results suggest that auto-amplification of Tie2 expression by treatment with COMP-Ang1 above a certain dose and exposure period could be one of the mechanisms. Once Tie2 expression is activated by a long-term and excess exposure to COMP-Ang1, after discontinuation of COMP-Ang1, the subsequent activation of Tie2 might be achieved by endogenous circulating Ang1 or increased shear stress caused by increased blood flow.[17] However, auto-amplification of Tie2 expression cannot be achieved below a certain dose and exposure period of COMP-Ang1, as evidenced by the experiments with intravenous administration of COMP-Ang1 recombinant protein. Therefore, the dose and the exposure period of COMP-Ang1 or VEGF should be considered in any therapeutic approaches where permanent vascular enlargements are needed to alleviate dysfunctions of ischemic tissues.

Tie1, an endothelial-specific receptor tyrosine kinase, shares a high degree of homology with Tie2. Although Tie1 was isolated more than a decade ago,[18] no ligand had been found to activate it. Recently, Saharinen et al demonstrated that COMP-Ang1 stimulated Tie1 phosphorylation in cultured endothelial cells.[19] Moreover, they showed that COMP-Ang1–induced Tie1 activation was amplified via Tie2 and was more efficient than native Ang1- and Ang4-induced Tie1 activation. Thus, COMP-Ang1 and Ang1 are now known to be activating ligands for both Tie1 and Tie2. However, our data indicate that COMP-Ang1–induced vascular remodeling in adult tracheal vessels is mainly mediated through activation of Tie2, not by Tie1. (See expanded Discussion section in the online data supplement.)

Although Ang1 induces vascular enlargement and has therapeutic benefits to ischemic tissues in several experimental animal models,[6,7,9] little is known about whether the vascular enlargement is accompanied by enhanced blood flow. Our results showed that COMP-Ang1–induced vascular enlargement was accompanied by enhanced tissue blood flow in the trachea. Therefore, enhanced blood flow through arteriolar and venular enlargements induced by COMP-Ang1 could provide a great therapeutic benefit to ischemic peripheral tissues. In fact, Ang1-induced vessel enlargement is a unique characteristic among many growth factors. Our immunohistological examination of phosphohistone H3 revealed that COMP-Ang1–induced vascular enlargements were evidently the result of endothelial proliferation, which is consistent with a recent report.[14] Thus, arteriolar and venular enlargements are achieved mainly by circumferential endothelial proliferation, which is a unique phenomenon and is different from multidirectional endothelial cell proliferation during vasculogenesis and angiogenesis. Moreover, our results revealed that different organs showed different sensitivities to long-term and sustained COMP-Ang1. In fact, blood vessels in the skin, heart, adrenal cortex, and liver, among other organs, are relatively sensitive to the COMP-Ang1–induced vascular enlargement. Therefore, COMP-Ang1 could provide a great therapeutic benefit to patients with delayed skin wound healing and ischemic heart diseases through its ability to promote vascular remodeling. Nevertheless, the mice treated with long-lasting and sustained COMP-Ang1 did not show any significant changes in body weight, systemic blood pressure, or heart rate. More detailed analysis will be necessary to clarify how it is possible that the mice with enlarged blood vessels caused by long-term and sustained COMP-Ang1 have normal blood pressure and heart rate.

Ang1 is known to be a strong growth factor for pericyte recruitment to nascent endothelial cells during development.[3–5] This Ang1-induced pericyte recruitment is related to the Ang1-induced antileakage effect on VEGF and proinflammatory stimuli.[5] However, our results show a lower number and poorer covering of pericytes in COMP-Ang1–

induced enlarged postcapillary venules. In fact, in a mouse model that completely blocks pericyte recruitment to developing vessels by injection of antagonistic monoclonal antibody against platelet-derived growth factor receptor-β, Angl is able to restore a hierarchical architecture of growing blood vessels and rescues retinal edema and hemorrhage even in the absence of pericyte recruitment.[20] Thus, COMP-Angl may be able to assemble endothelial cells in a frame of hierarchical architecture without pericyte recruitment in the COMP-Angl–induced enlarged blood vessels.

In conclusion, long-lasting vascular enlargement and enhancement of blood flow can be achieved by long-term and sustained exposure to COMP-Angl.

Acknowledgments

Supported, in part, by the Bio-Challenge Program and the National Research Laboratory Program (2004-02376 to G.Y.K.) of the Korean Ministry of Science and Technology, the Korea Health R&D Project (0405-DB01-0104-0006 to G.Y.K.), the Ministry of Health & Welfare, and the Korea Science and Engineering Foundation (R01-2004-000-10045-0 to B.H.J.). Also supported by National Institutes of Health grants HL-24136 and HL-59157 from the National Heart, Lung and Blood Institute (to D.M.D.).

References

1. Davis S, Aldrich TH, Jones PF, Acheson A, Compton DL, Jain V, Ryan TE, Bruno J, Radziejewski C, Maisonpierre PC, Yancopoulos GD. Isolation of angiopoietin-1, a ligand for the TIE2 receptor by secretion-trap expression cloning. *Cell*. 1996;87:1161–1169.
2. Dumont DJ, Gradwohl G, Fong GH, Puri MC, Gertsenstein M, Auerbach A, Breitman ML. Dominant-negative and targeted null mutations in the endothelial receptor tyrosine kinase, tek, reveal a critical role in vasculogenesis of the embryo. *Genes Dev*. 1994;8:1897–1909.
3. Suri C, Jones PF, Patan S, Bartunkova S, Maisonpierre PC, Davis S, Sato TN, Yancopoulos GD. Requisite role of angiopoietin-1, a ligand for the TIE2 receptor, during embryonic angiogenesis. *Cell*. 1996;87:1171–1180.
4. Suri C, McClain J, Thurston G, McDonald DM, Zhou H, Oldmixon EH, Sato TN, Yancopoulos GD. Increased vascularization in mice overexpressing angiopoietin-1. *Science*. 1998;282:468–471.
5. Thurston G, Suri C, Smith K, McClain J, Sato TN, Yancopoulos GD, McDonald DM. Leakage-resistant blood vessels in mice transgenically overexpressing angiopoietin-1. *Science*. 1999;286:2511–2514.
6. Shyu KG, Manor O, Magner M, Yancopoulos GD, Isner JM. Direct intramuscular injection of plasmid DNA encoding angiopoietin-1 but not angiopoietin-2 augments revascularization in the rabbit ischemic hindlimb. *Circulation*. 1998;98:2081–2087.
7. Chae JK, Kim J, Lim ST, Chung MJ, Kim WH, Kim HG, Ko JK, Koh GY. Co-administration of angiopoietin-1 and vascular endothelial growth factor enhances collateral vascularization. *Arterioscler Thromb Vasc Biol*. 2000;20:2573–2578.
8. Baffert F, Thurston G, Rochon-Duck M, Le T, Brekken R, McDonald DM. Age-related changes in vascular endothelial growth factor dependency and angiopoietin-1-induced plasticity of adult blood vessels. *Circ Res*. 2004;94:984–992.
9. Zhou YF, Stabile E, Walker J, Shou M, Baffour R, Yu Z, Rott D, Yancopoulos GD, Rudge JS, Epstein SE. Effects of gene delivery on collateral development in chronic hypoperfusion: diverse effects of angiopoietin-1 versus vascular endothelial growth factor. *J Am Coll Cardiol*. 2004;44:897–903.
10. Cho CH, Kammerer RA, Lee HJ, Steinmetz MO, Ryu YS, Lee SH, Yasunaga K, Kim KT, Kim I, Choi HH, Kim W, Kim SH, Park SK, Lee GH, Koh GY. COMP-Angl: a designed angiopoietin-1 variant with nonleaky angiogenic activity. *Proc Natl Acad Sci U S A*. 2004;101:5547–5552.
11. Hwang SJ, Choi HH, Kim KT, Hong HJ, Koh GY, Lee GM. Expression and purification of recombinant human angiopoietin-2 produced in CHO cells. *Protein Express Purif*. 2005;39:175–183.
12. Schlaeger TM, Bartunkova S, Lawitts JA, Teichmann G, Risau W, Deutsch U, Sato TN. Uniform vascular-endothelial-cell-specific gene expression in both embryonic and adult transgenic mice. *Proc Natl Acad Sci U S A*. 1997;94:3058–3063.
13. Baluk P, Raymond WW, Ator E, Coussens LM, McDonald DM, Caughey GH. Matrix metalloproteinase-2 and -9 expression increases in Mycoplasma-infected airways but is not required for microvascular remodeling. *Am J Physiol Lung Cell Mol Physiol*. 2004;287:L307–L317.
14. McDonald DM. Endothelial gaps and permeability of venules in rat tracheas exposed to inflammatory stimuli. *Am J Physiol*. 1994;266:L61–L83.
15. Cho CH, Kammerer RA, Lee HJ, Yasunaga K, Kim KT, Choi HH, Kim W, Kim SH, Park SK, Lee GM. A designed angiopoietin-1 variant, COMP-Angl, protects against radiation-induced endothelial cell apoptosis. *Proc Natl Acad Sci U S A*. 2004;101:5553–5558.
16. Dor Y, Djonov V, Abramovitch R, Itin A, Fishman GI, Carmeliet P, Goelman G, Keshet E. Conditional switching of VEGF provides new insights into adult neovascularization and pro-angiogenic therapy. *EMBO J*. 2002;21:1939–1947.
17. Lee HJ, Koh GY. Shear stress activates Tie2 receptor tyrosine kinase in human endothelial cells. *Biochem Biophys Res Commun*. 2003;304:399–404.
18. Partanen J, Armstrong E, Makela TP, Korhonen J, Sandberg M, Renkonen R, Knuutila S, Huebner K, Alitalo K. A novel endothelial cell surface receptor tyrosine kinase with extracellular epidermal growth factor homology domains. *Mol Cell Biol*. 1992;12:1698–1707.
19. Saharinen P, Kerkela K, Ekman N, Marron M, Brindle N, Lee GM, Augustin H, Koh GY, Alitalo K. Multiple angiopoietin recombinant proteins activate the Tie1 receptor tyrosine kinase and promote its interaction with Tie2. *J Cell Biol*. 2005;169:239–243.
20. Uemura A, Ogawa M, Hirashima M, Fujiwara T, Koyama S, Takagi H, Honda Y, Wiegand SJ, Yancopoulos GD, Nishikawa S. Recombinant angiopoietin-1 restores higher-order architecture of growing blood vessels in mice in the absence of mural cells. *J Clin Invest*. 2002;110:1619–1628.

THE JOURNAL OF BIOLOGICAL CHEMISTRY

Vol. 280, No. 6, Issue of February 11, pp. 5022–5031, 2005
Printed in U.S.A.

Local Activation of Rap1 Contributes to Directional Vascular Endothelial Cell Migration Accompanied by Extension of Microtubules on Which RAPL, a Rap1-associating Molecule, Localizes*[S]

Received for publication, August 24, 2004, and in revised form, November 23, 2004
Published, JBC Papers in Press, November 29, 2004, DOI 10.1074/jbc.M409701200

Hisakazu Fujita, Shigetomo Fukuhara, Atsuko Sakurai, Akiko Yamagishi, Yuji Kamioka, Yoshikazu Nakaoka, Michitaka Masuda, and Naoki Mochizuki‡

From the Department of Structural Analysis, National Cardiovascular Center Research Institute, Suita, Osaka 565-8565, Japan

Endothelial cell migration is promoted by chemoattractants and is accompanied with microtubule extension toward the leading edge. Cytoskeletal microtubules polarize to function as rails for delivering a variety of molecules by motor proteins during cell migration. It remains, however, unclear how directional migration with polarized extension of microtubules is regulated. Here we report that Rap1 controls the migration of vascular endothelial cells. We found that Rap1-associating molecule, RAPL, which belongs to the Ras association domain family (Rassf), localized on microtubules and that activated Rap1 induced dissociation of RAPL from microtubules. A Rap1 activation-monitoring probe based on the fluorescence resonance energy transfer enabled us to demonstrate that local Rap1 activation occurs at the leading edge of the cells under the two types of cell migration, chemotaxis and wound healing. Time lapse imaging of microtubules marked by enhanced green fluorescent protein-RAPL showed the directional growth of microtubules toward the leading edge of the migrating cells. Using adenovirus, inactivation of Rap1 by expression of rap1GAPII inhibited wound healing. In addition, disconnection of Rap1 and RAPL by expression of a RAPL mutant also perturbed wound healing. Collectively, the locally activated Rap1 and its association with RAPL controls the directional migration of vascular endothelial cells.

Rap1 belongs to the Ras GTPase family and cycles between a GDP-bound inactive form and a GTP-bound active form (1). Rap1 activation is regulated by guanine nucleotide exchange factor (GEF),[1] whereas Rap1 inactivation is regulated by GTPase-activating protein (GAP). GEFs contain a catalytic domain and regulatory domains that either bind to upstream molecules or are regulated by second messengers such as cAMP and Ca^{2+}. The former GEFs include C3G and PDZ-GEF; the latter includes CalDAG-GEFs and Epac (cAMP-GEF) (reviewed in Ref. 2). Thus, the spatial Rap1 activation depends on the localization of GEF and the spreading of second messengers. Like GEFs, the spatial Rap1 inactivation depends on the localization of GAPs for Rap1 (3). We have currently developed a spatio-temporal activation/inactivation monitoring probe for Rap1 in living cells (4).

Once activated by GEFs, GTP-bound Rap1 associates with effector molecules including Raf-1, B-Raf, RalGDS, and AF-6 (2). Rap1 shares these effector molecules with Ras protein; therefore, Rap1 is suggested to function antagonistically on the Ras-activated intracellular signaling pathway. However, Rap1 may have a unique function in regulating cell adhesion (5, 6). Rap1 was recently reported to be indispensable for cell-extracellular matrix (ECM) contacts by stabilizing the cell-ECM contacts, indicating that Rap1 enhances cell adhesion to ECM (7, 8). Moreover, Bud1, the yeast homologue of Rap1, determines the budding site (9), and Rap1 regulates adherens junction positioning for cell division in *Drosophila* (10), implying that Rap1 is also involved in cell polarization.

Cells have a polarity determined by cell protrusions and retractions, when moving toward certain chemoattractants or during wound healing. In the protrusions, actin is actively polymerized and depolymerized, whereas in retractions stabilized actin fibers are observed (11). For perpetual moving toward the chemoattractants, asymmetrical polarity of cell contacts to ECM is required. Focal adhesions connecting actin stress fibers are assembled in the protrusions and disassembled in the retractions of migrating cells (reviewed in Ref. 12). Like actin, microtubules are assembled toward the leading edge of the protrusions. By constituting rails for motor proteins carrying the molecules to the protrusive part of the cell, microtubule promotes cell polarity (13). Furthermore, recently, assembly and disassembly of focal adhesions are reportedly regulated by microtubules (14, 15). Thus, microtubule extension toward the leading edge parallels the change in polarity of the motile cells toward the chemoattractants or during wound healing.

* This work was supported by grants from the Ministry of Health, Labor, and Welfare of Japan; from the Promotion of Fundamental Studies in Health Science of the Organization for Pharmaceutical Safety and Research of Japan; from the Ministry of Education, Science, Sports and Culture of Japan; from the Cell Science Research Foundation; and from the Mochida Memorial Foundation for Medical and Pharmaceutical Research. The costs of publication of this article were defrayed in part by the payment of page charges. This article must therefore be hereby marked "*advertisement*" in accordance with 18 U.S.C. Section 1734 solely to indicate this fact.

[S] The on-line version of this article (available at http://www.jbc.org) contains two additional figures and eight videos.

‡ To whom correspondence should be addressed: Dept. of Structural Analysis, National Cardiovascular Center Research Institute, 5-7-1 Fujishirodai, Suita, Osaka 565-8565, Japan. Tel.: 81-6-6833-5012 (ext. 2508); Fax: 81-6-6835-5461; E-mail: nmochizu@ri.ncvc.go.jp.

[1] The abbreviations used are: GEF, guanine nucleotide exchange factor; CFP, cyan fluorescent protein; ECM, extracellular matrix; EGFP, enhanced green fluorescent protein; FRET, fluorescence resonance energy transfer; GAP, GTPase-activating protein; GFP, green fluorescent protein; GST, glutathione *S*-transferase; HAEC, human aortic endothelial cell; HUVEC, human umbilical vein endothelial cell; MTOC, microtubule-organizing center; Rassf, Ras association domain family; S1P, sphingosine 1-phosphate; SDF-1, stromal-derived factor-1; YFP, yellow fluorescent protein; MES, 4-morpholineethanesulfonic acid.

RAPL/NORE1B (hereafter referred to as RAPL) is identified as a Rap1-binding molecule (16), which contains a Ras/Rap1 binding domain and belongs to the Ras association domain family (Rassf) (17, 18). Whereas Rassf members function as potent suppressors of tumors (19–21), RAPL links Rap1 activation upon T cell receptor cross-linking and stromal-derived factor-1 (SDF-1) stimulation to integrin activation. In addition, RAPL mediates the polarized distribution of SDF-1 receptors upon Rap1 activation (16). Recently, Rassf1 has been shown to localize at and stabilize microtubules (22). However, it is unclear whether other molecules belonging to Rassf function in the association with Ras family GTPases.

We investigate the localization of RAPL in the vascular endothelial cells and how Rap1-RAPL participates in determining the directional migration in response to a chemoattractant, sphingosine 1-phosphate (S1P) (23), and during wound healing. RAPL localizes at the microtubule-organizing center (MTOC) and microtubules. Rap1 is activated at the leading edge of migrating cells. In addition, inactivation of Rap1-RAPL signal perturbed the wound closure. These data suggest that local activation of Rap1 and its association with RAPL regulates the directional cell migration of vascular endothelial cells.

EXPERIMENTAL PROCEDURES

Reagents and Antibodies—S1P was purchased from Biomol (Plymouth, PA). Protein A-Sepharose was from Calbiochem. Anti-green fluorescent protein (GFP) was developed in our laboratory. Anti-β-tubulin, anti-γ-tubulin, and anti-FLAG (M2) were purchased from Sigma, and anti-Rap1 was from BD Biosciences. Anti-RAPL antibody was a kind gift from T. Kinashi (Kyoto University, Japan).

Plasmids—The coding sequences of human Rassf1A, Rassf1C, Rassf2 (KIAA0168), Rassf3, and RAPL (NORE1B) were amplified by PCR using human heart cDNA library as a template. pCA-EGFP-Rassf1A, -Rassf1C, -Rassf2, -Rassf3, and RAPL were derived from pCAGGS eukaryotic expression vector and expressed enhanced green fluorescent protein (EGFP)-tagged each Rassf molecules (24). cDNAs encoding RAPL deletion mutants as indicated in Fig. 4 were amplified by PCR and ligated into pCA-EGFP vector similarly to Rassf1. dC1, dC2, dC3, and dN encoded amino acids 1–222, 1–168, 1–100, and 101–265 of RPAL, respectively. A mutant of RAPL (hereafter referred to as the RA mutant), in which Lys^{123}, Arg^{124}, Lys^{135}, Lys^{154}, Lys^{155}, Asp^{160}, and Asn^{161} were replaced with Ala, was reported to be incapable of associating with Rap1 (16). cDNA encoding an RA mutant was amplified by PCR-based mutagenesis and subcloned into pCA-EGFP. pCXN2-FLAG-Rap1 expressed FLAG-tagged Rap1. Either constitutive active or dominant negative forms of Rap1 (Rap1V12 or Rap1N17) cDNAs were similarly inserted into pCXN2-FLAG. pIRM21-Rap1V12 expressed FLAG-tagged Rap1V12 and internal ribosomal entry site-driven dsFP593 as described previously (24). pIRM21-rap1GAPII expressed both FLAG-tagged rap1GAPII and internal ribosomal entry site-driven dsFP593. pCA-DsRed-CrkI was derived from pCAGGS eukaryotic expression vector as described previously (24). pRaichu-Rap1, a Rap1 activation monitoring probe based on fluorescence resonance energy transfer (FRET), was described previously (4). pRaichu-Rap1 expressed a chimeric protein consisting of yellow fluorescent protein (YFP), Rap1, and Ras-binding domain of Raf and cyan fluorescent protein (CFP) followed by the CAAX motif of Ki-Ras. In pRaichu-Rap1N17, a cDNA encoding Rap1N17 was replaced with that encoding Rap1. pGEX-RAPL was constructed by inserting a cDNA encoding full-length RAPL into pGEX (Amersham Biosciences).

Adenovirus—Both an adenovirus-expressing EGFP-tagged RAPL and an adenovirus-expressing EGFP-tagged RA mutant of RAPL were produced using the Adeno-X expression system (BD Biosciences). Briefly, cDNA from pCA-EGFP-RAPL was inserted into Adeno-X viral DNA using pShuttle as a transfer vector. Adenovirus-expressing EGFP-RAPL was produced from HEK293 cells transfected with Adeno-X-EGFP-RAPL. An adenovirus-expressing RA mutant of RAPL was produced in a similar manner to RAPL-expressing adenovirus. The EGFP-expressing adenovirus and the rap1GAPII-expressing adenovirus were generous gifts from H. Kurose (Kyushu University, Japan) and S. Hattori (Tokyo University, Japan), respectively.

Cell Culture and Transfection—Human umbilical vein endothelial cells (HUVECs) and human aortic endothelial cells (HAECs) were purchased from Cascade Biologics, Inc. (Portland, OR) and cultured in Humedia-EG2 as previously reported (24). HEK293T cells were generous gifts from Dr. B. J. Mayer (University of Connecticut) and maintained as described previously. Jurkat cells and HEK293 cells were obtained from the American Type Culture Collection (Manassas, VA) and cultured in RPMI 1640 (Invitrogen) and Dulbecco's modified Eagle's medium supplemented with 10% fetal bovine serum. Cultured cells were transfected using Lipofectamine 2000 reagent (Invitrogen).

Reverse Transcription-PCR, Pull-down Assay, Immunoprecipitation, and Immunoblotting—RNAs from cultured Jurkat cells and HUVECs were prepared by TRIzol (Invitrogen). cDNAs was synthesized by reverse transcriptase reaction using random primer and RNAs as templates. The cDNA specific for human RAPL was amplified by PCR using a primer set (5′RAPL, CTGGACGAGGAACTGGAAGACTGCTTC; 3′RAPL, AGGGATGGAGAAGGCATCCCACTCTAC). GTP-bound Rap1 was detected according to the method of Bos and co-workers (25). Briefly, HUVECs stimulated with 1 μM S1P for the time indicated at the *top* of Fig. 5 were lysed in lysis buffer (50 mM Tris, pH 7.5, 150 mM NaCl, 5 mM $MgCl_2$, 1% Nonidet P-40, 0.1% SDS, 0.5% deoxycholic acid, 1 mM Na_3VO_4). Precleared lysates were incubated with GST-Rap1-binding domain of RalGDS and glutathione-Sepharose beads. Proteins collected on the beads were subjected to SDS-PAGE followed by immunoblotting with anti-Rap1 antibody. Immunoprecipitation and immunoblotting were performed as described previously (26). Briefly, HEK293T transfected with plasmids as indicated in Fig. 1 were lysed using lysis buffer. Lysates were precleared by centrifugation at 15,000 × *g* for 10 min, followed by immunoprecipitation using anti-GFP and Protein A-Sepharose. Immunoprecipitates were subjected to SDS-PAGE and immunoblotting with anti-FLAG antibody and peroxidase-conjugated goat anti-mouse IgG as a primary and a secondary antibody, respectively. Proteins reacting with anti-FLAG were visualized by an ECL system (Amersham Biosciences) and an LAS-1000 system (Fuji Film, Japan).

Microtubule Binding Assay—Microtubule-associating protein-containing microtubule prepared from bovine brain were gifts from N. Yamagishi (Kyoto Pharmaceutical University, Japan). Glutathione *S*-transferase-fused RAPL (GST-RAPL) expressed in BL21-Star bacteria (Invitrogen) was collected on glutathione-Sepharose (Amersham Biosciences). GST-RAPL was eluted using 10 mM glutathione, precleared by centrifugation at 400,000 × *g*, and polymerized in microtubule-binding buffer (100 mM MES-KOH (pH 6.8), 2 mM EDTA, 1 mM $MgCl_2$, 10 mM Taxol, 4 M glycerol, and 1 mM GTP). For the microtubule binding assay, 5 μg of purified microtubules and GST-RAPL at the concentration indicated in Fig. 3 legend were mixed in 200 μl of microtubule-binding buffer for 30 min at 37 °C. After centrifugation at 400,000 × *g* for 15 min, equal amounts of the supernatant and the pellet were analyzed by SDS-PAGE and immunoblotting with anti-GST. Bovine serum albumin fraction V was used as a negative control for GST-RAPL.

Wound Healing Assay and Responses to Chemoattractant from a Micropipette—HUVECs or HAECs transfected with plasmids indicated in the figures were cultured on 35-mm glass bottom dishes coated with collagen until they reached the monolayer state. The cells were scratched by a regular 20-μl pipette tip along the diameter of the bottom glass. The culture medium remained unchanged during wound healing. Monolayer-cultured HUVECs infected with an adenovirus expressing rap1GAPII, an adenovirus expressing EGFP-RAPL, or an adenovirus expressing the RA mutant of RAPL were scratched and time lapse-imaged. HAECs expressing EGFP-RAPL or those expressing Raichu-Rap1 cultured on glass-bottom dishes coated with collagen were exposed to 1 μM S1P supplied by a micropipette (FemtoJet; Eppendorf Japan).

Fluorescence Microscopy and Confocal Imaging—HUVECs or HAECs transfected with plasmids expressing fluorescence-tagged proteins as indicated in the figure legends were imaged on an Olympus IX-81 inverted microscope. The microscope with a 75-watt xenon arc lamp was equipped with a cooled charge-coupled device camera, CoolSNAP-HQ (Roper Scientific), and two filter exchangers, controlled by MetaMorph 5.0 software (Molecular Devices). The EGFP image and DsRed image were obtained through an XF2043 dichroic filter (Omega) and either a set of an S484/15 excitation filter and an S515/30 emission filter or a set of an S555/25 excitation filter and an S630/60 emission filter, respectively, as reported previously (27). HUVECs transfected with pCA-EGFP-RAPL cultured on a collagen-coated glass-base dish were fixed by 4% paraformaldehyde at room temperature, followed by permeabilization with 0.1% Triton X-100. Permeabilized cells were incubated with anti-β-tubulin or anti-γ-tubulin antibody. Immunopositive reaction was visualized with Alexa 546 goat-anti-mouse IgG (Molecular Probes, Inc., Eugene, OR). Confocal images of EGFP and Alexa 546 were obtained by an Olympus BX50WI microscope controlled by Fluoview. To monitor the cell shape and localization of fluorescence-tagged molecules in living cells, a phase-contrast image and a fluo-

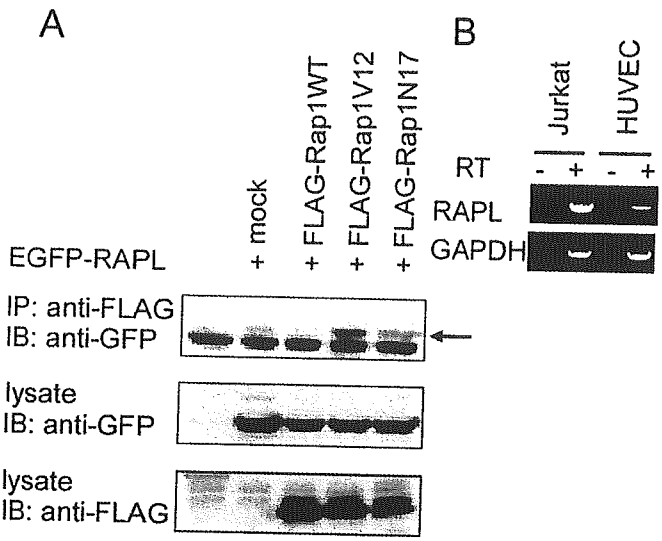

FIG. 1. **The association of RAPL with Rap1 and its expression in vascular endothelial cells.** *A*, HEK293T cells were transfected with plasmids as indicated at the *top*. Cell lysates were subjected to immunoprecipitation (*IP*) followed by immunoblotting (*IB*) with antibodies as indicated on the *left* or directly subjected to SDS-PAGE followed by immunoblotting with the antibodies as indicated on the *left*. An *arrow* denotes GTP-bound Rap1 co-immunoprecipitated with EGFP-tagged RAPL. *B*, RNA prepared from the cells as indicated at the *top* was subjected to reverse transcription-PCR analysis. The sequence of RAPL-specific primers is described under "Experimental Procedures." RNA from Jurkat cells was used as a positive control. The results are representative of more than three independent experiments.

rescence image were obtained every 20 s. A series of time lapse images were converted into video format using MetaMorph 5.0.

Imaging of Rap1 Activation in Living Cells—HAECs cultured on collagen-coated 35-mm diameter glass base dishes were transfected with pRaichu-Rap1 and observed after scratching. Cells similarly transfected with pRaichu-Rap1 were observed during exposure to 1 μM S1P supplied by a micropipette. The structure of Raichu-Rap1 and the principle of FRET is illustrated as in Fig. 5*D*. Cells were imaged on an Olympus IX-81 inverted fluorescence microscope in a method similar to fluorescence imaging as described previously (24). Dual images for CFP and YFP were obtained through an XF1071 excitation filter, an XF2034 dichroic filter, and an XF3075 emission filter for CFP and an XF3079 for YFP (Omega), respectively. The ratio image of YFP/CFP were created by MetaMorph 5.0 software and displayed as an intensity-modulated display image as described previously (4).

RESULTS

A Rap1-binding Protein, RAPL, Is Expressed in Vascular Endothelial Cells—RAPL associates with Rap1 upon T-cell receptor stimulation or chemokine stimulation, resulting in redistribution of integrin in lymphocytes (16). Vascular endothelial cells and hematopoietic cells originate from common hemangioblasts; therefore, we tested whether vascular endothelial cells express RAPL, since Jurkat cells express RAPL (16). RAPL expression was examined by reverse transcription-PCR analysis using a RAPL-specific primer set. HUVECs expressed RAPL mRNA similarly to Jurkat cells used as a positive control (Fig. 1*A*). We further examined the association of GTP-Rap1 with RAPL by the co-immunoprecipitation assay using 293T cells (Fig. 1*B*).

A member of Rassf1A localizes to microtubules in COS cells (22), whereas the localization of RAPL has not yet been clearly demonstrated, although it is reported to accumulate at the leading edge of T lymphocytes (16). Thus, we tested the localization of RAPL in the vascular endothelial cells by using EGFP-tagged RAPL. Rassf members as listed (Fig. 2*A*) were tagged with EGFP and expressed in HAECs. All Rassf members contain the Ras- and Rap1-binding domain (RA domain) (Fig. 2*A*). The expression of EGFP-tagged Rassfs was confirmed by the immunoblot analysis from the lysates of HEK293T cells transfected with the plasmids as indicated at the *top* (Fig. 2*B*). EGFP-tagged Rassf1A and -1C, splicing variants from the same gene, were found as circular fibers in the central region of cells except the nucleus, whereas EGFP-tagged Rassf3 and EGFP-RAPL were found as fibers emanating from the central to the periphery. These results suggested that the circular fibers on which EGFP-tagged Rassf1A and -1C localized may represent microtubules deformed by Rassf1-induced stabilization, as previously demonstrated (22). Rassf3 and RAPL appeared to localize on normal microtubules originating from MTOC to the periphery. Thus, we examined the colocalization of EGFP-RAPL with β-tubulin-constituting microtubules and with γ-tubulin preferably localized on MTOC. As expected, EGFP-RAPL clearly localized on microtubules from the MTOC to the periphery (Fig. 2*D*). In clear contrast to these fibrous expressions, EGFP-Rassf2 was found exclusively in the nucleus. We compared the EGFP-RAPL with EGFP-Rassf1A expressed in motile vascular endothelial cells using time lapse imaging. Both RAPL-expressing cells and Rassf1A-expressing cells showed membrane ruffling (Supplemental Video 1); however, microtubules marked by EGFP-RAPL moved dynamically as regular microtubules, whereas those marked by EGFP-Rassf1 were static (Supplemental Video 2). These data indicated that Rassf members, Rassf3 and RAPL, appear to bind to microtubules without affecting the endogenous microtubule structure.

We further confirmed the localization of RAPL on microtubules by immunostaining using anti-RAPL antibody. Endogenous RAPL localized on microtubules in HAECs (Fig. 3*A*). The association of RAPL and microtubules were examined by biochemical analysis using purified microtubules and GST-RAPL. The microtubule binding assay revealed that GST-RAPL cosedimented with microtubules in a concentration-dependent manner. Although GST-RAPL and tubulin closely migrated in SDS-PAGE (Fig. 3*B*, *top panel*), GST-RAPL was clearly separated by immunoblotting with anti-GST (Fig. 3*B*, *middle panel*). In agreement with these observations, when microtubule formation was inhibited by nocodazole, the filamentous expression of RAPL was not observed (Supplemental Fig. 1). Collectively, these results indicated that endogenous RAPL localizes on microtubules in vascular endothelial cells.

RAPL Requires Rap1-associating Domain for Localizing on Microtubules but Not Its Association with Rap1—To define the region responsible for the association of RAPL with microtubules, we constructed a series of truncated mutants and a mutant incapable of associating with Rap1 (RA mutant) (Fig. 4*A*). The expression of EGFP-tagged RAPL and its mutants was confirmed by the immunoblot analysis from the lysates of HEK293T cells transfected with the plasmids as indicated at the *top* of Fig. 4*B*. We examined the expression of EGFP-tagged RAPL and its mutants in HAECs (Fig. 4*C*). EGFP-tagged full-length RAPL and coiled-coil domain-lacking mutant (dC1) localized on microtubules. Intriguingly, RA mutant also localized on microtubules. However, neither RA domain-lacking mutant (dC2 and dC3) nor a mutant lacking the amino-terminal 100 amino acids (dN) localized on microtubules. The EGFP-tagged RA domain alone was not expressed on the microtubules. These data indicated that the association of RAPL with Rap1 is not required for the localization of RAPL on microtubules and that the amino-terminal part of RAPL and the RA domain are essential for its targeting to microtubules.

Rap1 Locally Activated by S1P Triggers Directional Migration Preceding Microtubule Extension—To understand the significance of Rap1 activation and RAPL localizing on microtubules, we examined RAPL localization in HAECs expressing either Rap1V12 or rap1GAPII. EGFP-RAPL dislocated from microtu-

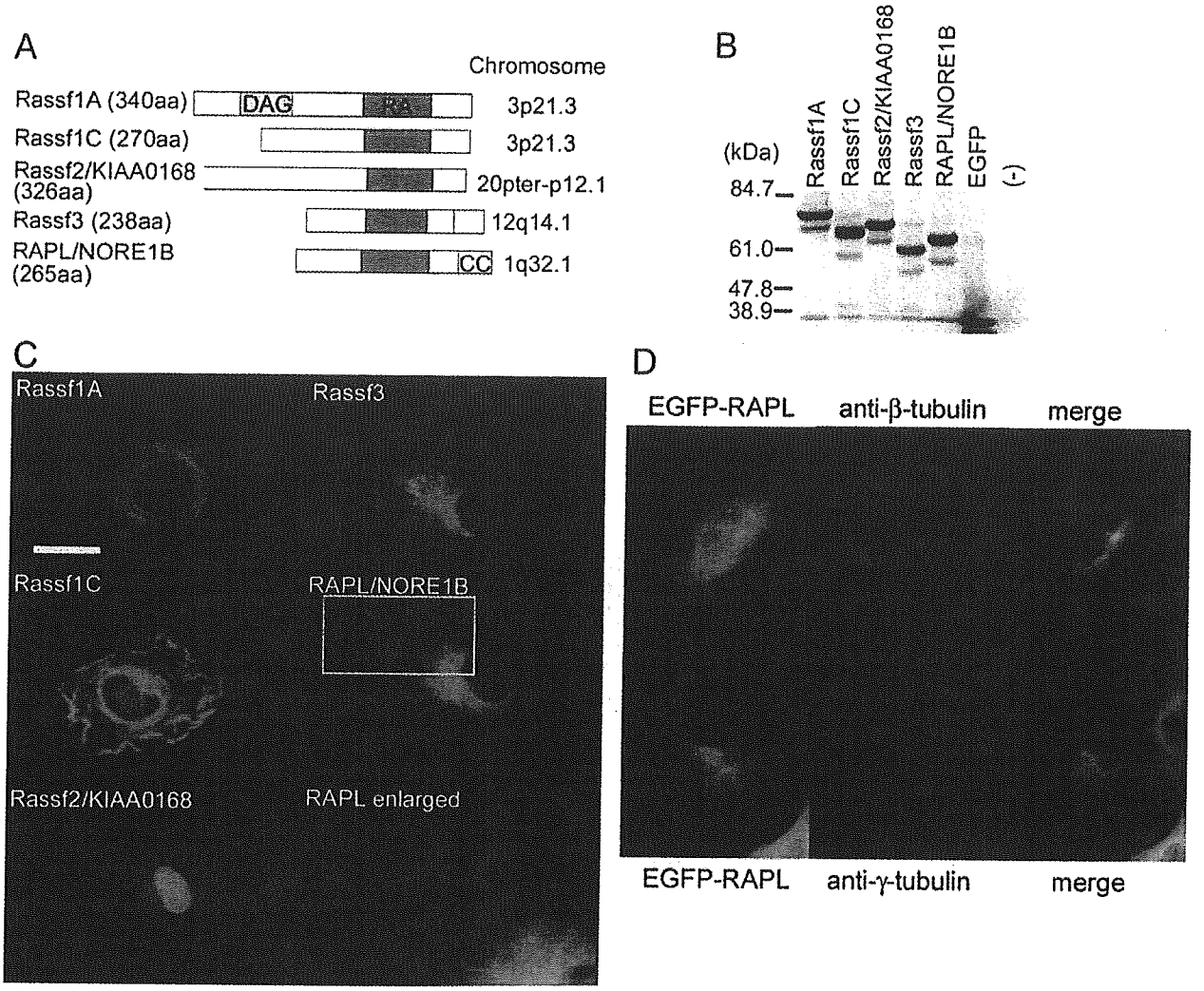

FIG. 2. **RAPL localizes to the microtubules in vascular endothelial cells.** *A*, Rassf members are schematically illustrated. All Rassfs contain a Ras/Rap1-associating domain (*RA*). Only Rassf1A contains the diacylglycerol-binding motif (*DAG*). Rassf3 and RAPL have coiled-coil domain (*CC*) in the carboxyl terminus. The localization of each gene to human chromosome is indicated on the *right*. *aa*, amino acids. *B*, HEK293T cells were transfected with EGFP-tagged plasmids as indicated at the *top*. Cell lysates were subjected to SDS-PAGE followed by immunoblotting with anti-GFP. −, untransfected. Molecular weight markers are indicated on the *left*. *C*, HAECs were transfected with the plasmids used in *B* and imaged through an Olympus IX81 fluorescent microscope. Note that EGFP-tagged Rassf1A and Rassf1C localize on the spiral fibers, whereas EGFP-tagged Rassf3 and RAPL localize at fibrous structures emanating from the center of the cell to the periphery. The tubular structure observed in HAECs expressing EGFP-RAPL is enlarged in the *right bottom panel*. Motile HAECs transfected with either EGFP-Rassf1A or EGFP-Rassf3 were video-imaged for phase contrast and EGFP. A series of phase-contrast images and EGFP images of each cell were converted to two videos, Supplemental Video 1 (phase contrast) and Supplemental Video 2 (EGFP). Elapsed time in video is indicated as h: min. Noticeably, the spiral structure surrounding the nucleus in the cell expressing Rassf1A does not move in the protrusive area at all. In clear contrast, the array from the center to the periphery of the cell expressing EGFP-Rassf3 moves toward the ruffled membrane, although both cells move spontaneously, similar to the untransfected cells. *Bar*, 20 μm. *D*, HAECs expressing EGFP-RAPL plated on a collagen-coated glass base dish were fixed with 4% paraformaldehyde, permeabilized with 0.1% Triton X-100, and incubated with anti-β-tubulin (*top*) or anti-γ-tubulin (*bottom*). Immunoreactive proteins were visualized by Alexa546 goat anti-mouse IgG. Both EGFP and Alexa546 images obtained through a BX50WI confocal microscope controlled by Fluoview are shown as RAPL (*green*), tubulin (*red*), and superimposed (*merge*). Note that EGFP-RAPL localizes on microtubules from the MTOC to the peripheral microtubules. *Bar*, 20 μm.

bules in HAECs expressing Rap1V12, whereas it localizes on microtubules in HAECs expressing rap1GAPII (Fig. 5*A*). These results suggested that activated Rap1 appears to determine the localization of RAPL. Thus, we investigated the effect of local activation of Rap1 on localization of EGFP-RAPL. Since vascular endothelial cells become motile upon S1P stimulation, S1P is thought to function as a chemoattractant (23). S1P did activate Rap1 as demonstrated by pull-down assay (Fig. 5*B*). GTP-Rap1 was increased at 1 min after S1P stimulation, and its activation persisted until 15 min after stimulation.

To examine the orientation of microtubule growth upon local S1P stimulation, we applied S1P to HAECs using micropipette. HAECs expressing EGFP-RAPL were monitored for cell movement and microtubule growth by phase-contrast and EGFP observations, respectively. HAECs cultured on the collagen-coated dish spontaneously moved around and exhibited prominent membrane ruffling, where the microtubules marked by EGFP-RAPL grew forward as shown by the *center panels* of Fig. 5*C*. The same cell was stimulated by 1 μM S1P released from the micropipette tip (Fig. 5*C*, *right panel*). The cell changed the direction of movement and showed remarkable membrane ruffles toward the pipette tip in response to S1P. Notably, microtubules marked by EGFP-RAPL started to grow in the protrusive area in the U-turned cell. The responses to S1P were constantly observed when HAECs were exposed to S1P from the tip of the micropipette. A series of phase-contrast images and EGFP images were converted to a video (Supplemental Video 3). We further confirmed the requirement of

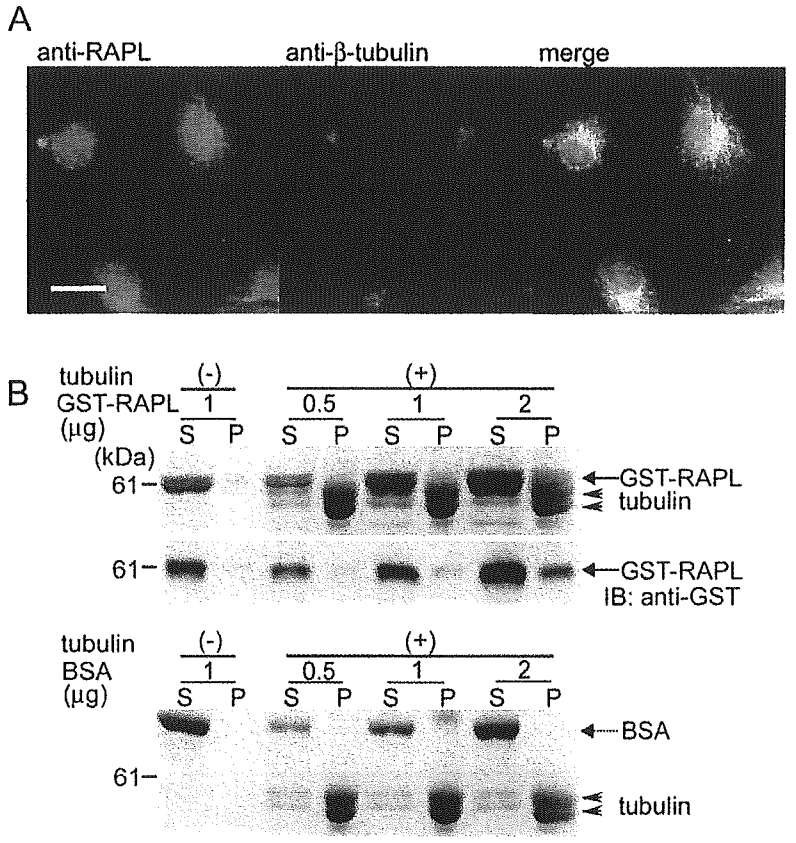

FIG. 3. **RAPL localizes on and binds to microtubules.** *A*, HAECs were immunostained with anti-RAPL antibody (*green*). Microtubules were visualized with immunostaining with anti-β-tubulin (*red*). A *merged image* is shown in the *right panel* (*merge*). *Bar*, 20 μm. *B*, GST-RAPL at the concentration as indicated at the *top* was mixed with 5 μg of purified tubulin (+) or without tubulin (−). After centrifugation at 400,000 × *g* for 30 min at 37 °C, supernatant (*S*) and pellet (*P*) were subjected to SDS-PAGE (*top panel*) followed by immunoblotting (*IB*) with anti-GST (*middle panel*). *Arrows*, *arrowheads*, and a *broken arrow* indicate GST-RAPL, tubulin, and bovine serum albumin (*BSA*), respectively. Note that GST-RAPL cosedimented with microtubules is detected in the pellet. To examine the specificity of the cosedimentation of GST-RAPL with microtubules, bovine serum albumin was used as a negative control in similar analyses to GST-RAPL (*bottom panel*).

microtubule growth for directional migration by examining whether endothelial cells extend membranes in response to S1P in the presence or absence of nocodazole. Before the nocodazole treatment, endothelial cells responded to S1P and extended their membranes, whereas after nocodazole, the cells did not extend their membranes (Supplemental Video 4). These data indicated that microtubules grow toward the chemoattractant, which promotes the directional cell movement.

To monitor the spatio-temporal activation of Rap1 in response to S1P from a micropipette, HAECs expressing Raichu-Rap1 were subjected to time lapse FRET imaging. Raichu-Rap1 consists of YFP, Rap1, the Ras-binding domain of Raf, CFP, and a CAAX box of Ki-Ras. This probe enabled us to show Rap1 activation by the increased ratio of YFP/CFP, based upon FRET from CFP to YFP (Fig. 5*D*). Raichu-Rap1-expressing HAECs exhibited remarkable membrane ruffles when stimulated with S1P from a micropipette (Fig. 5*E*, *third column*, *top*). At this time point, the increased FRET reflecting Rap1 activation was observed at the ruffled membrane (Fig. 5*E*, *third column*, *bottom*). When S1P was released from the relocated micropipette tip, the same cell responded to S1P and showed membrane ruffles toward the micropipette, similar to the first test. The similar Rap1 activation demonstrated by increased FRET was observed at the ruffled membrane (Fig. 5*E*, *right column*). A video image for both phase-contrast view and that for FRET images is shown as Supplemental Video 5. Rap1 activation at the ruffled membrane upon S1P stimulation was confirmed by the observation that Rap1 was not activated at the ruffled membrane before the S1P stimulation (Supplemental Fig. 2*A*). In addition, FRET observed at the ruffled membrane using Raichu-Rap1 was not detected when Raichu-Rap1N17 was used, although S1P-induced membrane ruffling was observed (Supplemental Fig. 2*B* and Video 6). By stimulating cells with S1P-free medium, we also excluded the possibility that fluid pressure or the proximity of the pipette tip to the cell might cause FRET (Supplemental Video 7). These data indicated that chemoattractant-induced local activation of Rap1 may become a trigger of directional migration accompanied by extension of EGFP-RAPL-marked microtubules.

Rap1 Activated during Wound Healing Is Accompanied by Microtubule Extension—To assess the consequence of the Rap1 activation and the association of activated Rap1 with RAPL, we examined the activation of RAPL and EGFP-RAPL-marked microtubules during wound healing. Microtubules grow in the protruding region of motile polarizing fibroblasts (28). It has been unclear what determines the polarized growth of microtubules. During wound healing, monolayer vascular endothelial cells migrated to the wound unidirectionally (Fig. 6*A*, *top panels*, phase-contrast observations). Crk is an adaptor protein linking signaling from integrins as well as receptor tyrosine kinases to its Src homology 3 domain-binding proteins via Src homology 2 domain. It localizes at focal adhesions by constituting complexes with Src homology 2 domain-binding partners, paxillin and p130Cas (29, 30). To monitor the focal adhesion assembly and growth of microtubules simultaneously, endothelial cells were transfected with the plasmids expressing DsRed-CrkI and EGFP-RAPL. Before scratching, DsRed-CrkI was punctually expressed in the focal adhesions at the cell periphery and the cell body (Fig. 6*A*, *bottom*, *left panel*). When cells started to move toward the wound, the focal complexes and focal adhesions marked by DsRed-CrkI developed profoundly in the leading edge of the cells (24, 31); meanwhile, those in the retracting region were disassembled (Fig. 6*A*, *bottom*, *right panel*). During cell migration upon scratching, microtubules marked by EGFP-RAPL grew in the protrusive region and developed toward the leading edge marked by DsRed-CrkI (Fig. 6*A*). A series of images for microtubules marked by EGFP-RAPL and those for focal adhesions marked by DsRed-CrkI were converted to a video file (Supplemental Video 8). We further confirmed that endogenous RAPL localized on microtubules in the protruding area of migrat-

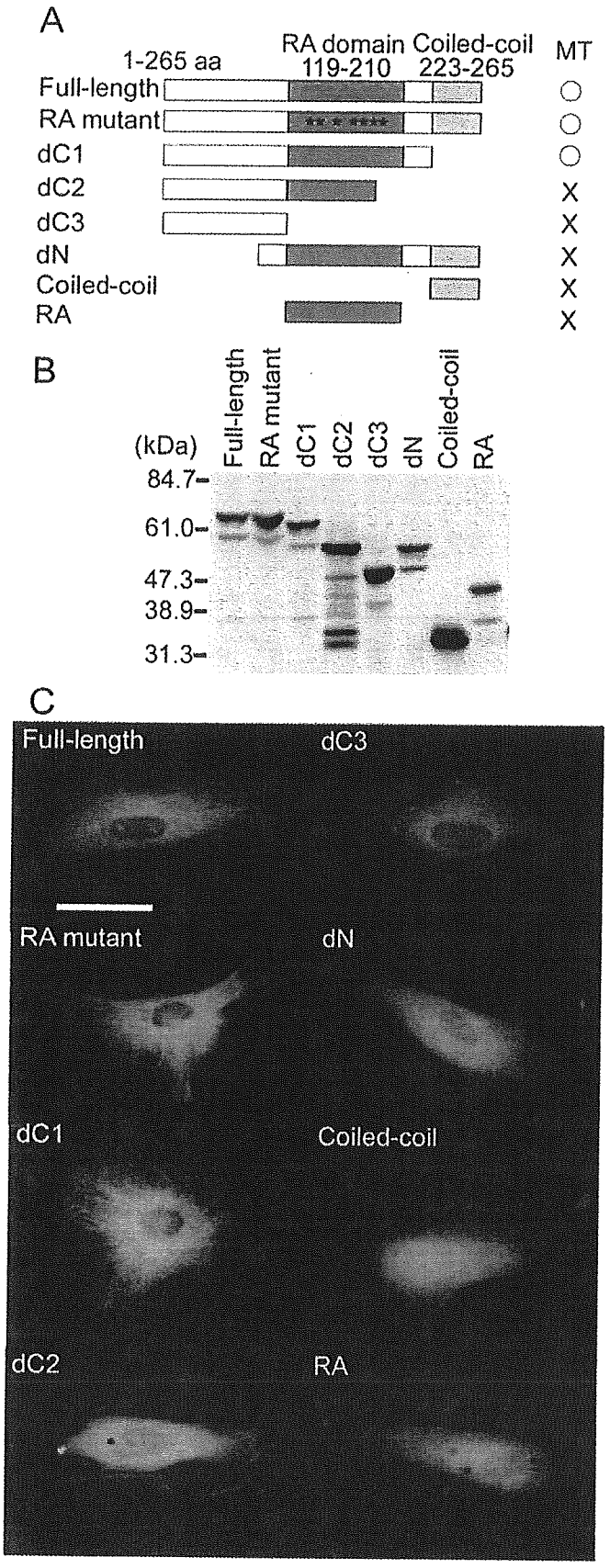

FIG. 4. **The sequence besides the essential amino acids in RA domain required for the association of RAPL with Rap1 is necessary for the localization of RAPL to microtubules.** *A*, schematic illustration of RAPL and its mutants. RAPL consists of an uncharacterized amino terminus, followed by a Ras/Rap1-associating domain (RA domain) and coiled-coil domain. The amino acid (*aa*) number encoding each domain is indicated at the *top*. *RA mutant*, the mutant incapable of associating with Ras and Rap1. The *stars* indicate the seven amino acids required for the association of RAPL with Rap1 that are replaced with Ala. dC1 and dC2 lacks the coiled-coil domain and both the RA domain and the coiled-coil domain, respectively. dC3 consists of the amino-terminal 100 amino acids. dN lacks the amino-terminal 100 amino acids, which have not been characterized. The coiled-coil and the RA consist of the only coiled-coil domain and the RA domain, respectively. The localization of RAPL and its mutants on microtubules is summarized on the *right*. *B*, HEK293T cells were transfected with the plasmids encoding amino-terminally EGFP-tagged DNA, as indicated at the *top*. Cell lysates were subjected to SDS-PAGE, followed by immunoblot probed with anti-GFP antibody. Molecular weight markers are indicated at the *left*. *C*, HAECs transfected with the plasmids used in *B* were imaged using an Olympus IX-81 fluorescent microscope. Note that RA mutant and dC1 localize on microtubules as well as full-length RAPL. *Bar*, 40 μm.

ing cells during wound healing (Fig. 6*B*).

Rap1 is activated downstream of Crk via its Src homology 3 domain-binding protein, C3G, which is a GEF for Rap1 (32). Thus, we examined whether Rap1 was activated during cell migration using Raichu-Rap1. HAECs cultured as a monolayer sheet were transfected with plasmids expressing Raichu-Rap1 and time lapse-imaged under the phase-contrast and FRET view after scratching. Cells were moving into the wound as revealed by phase-contrast observations (Fig. 7, *left panels*). Cell expressing Raichu-Rap1 as well as untransfected cells moved toward the wound. Rap1 was activated at the membrane ruffles in the leading edge (Fig. 7, *right panels*), where Crk was localized at focal complexes or growing focal adhesions (Fig. 6). These results suggested that Crk-Rap1 signaling upon focal adhesion assembly may contribute to the directional migration.

Rap1-RAPL Signaling Is Required for Directional Movement during Wound Healing—To test whether Rap1 is required for wound healing, we examined the effect of inactivation of Rap1 by overexpression of rap1GAPII on the directional cell migration. Rap family consists of Rap1A, Rap1B, Rap2A, and Rap2B (1). These molecules share common GEFs and GAPs for their activation and inactivation, respectively. To examine the effect of the Rap family on wound healing, inactivation of Rap by rap1GAPII, a common GAP for all of the Rap family members (33), is preferable rather than knocking down these Rap molecules using the small interfering RNA technique. In addition, rap1GAPII is suitable for the inactivation of Rap1, because it is reported that Rap1N17 does not work as a dominant negative form of Rap1 (34). HUVECs cultured as a monolayer were infected with adenovirus expressing either EGFP or rap1GAPII for 24 h. Infection efficiency exceeded 90%, as confirmed by fluorescence microscopy (Fig. 8*C*). There was no difference in cell confluence between HUVECs expressing rap1GAPII and those expressing EGFP. The EGFP-expressing cells separated by the wound moved toward the center line of the wound, whereas rap1GAPII-expressing HUVECs did not. The wound was almost closed by mobilized EGFP-expressing HUVECs 24 h after scratching, whereas it was not closed by rap1GAPII-expressing HUVECs (Fig. 8*A*).

To test the requirement of Rap1-RAPL signaling for directional movement, we used the RA mutant of RAPL to interfere with the association of RAPL with Rap1. HUVECs expressing EGFP-RA mutant were compared with those expressing EGFP-RAPL during wound healing. HUVECs infected with EGFP-RAPL-expressing adenovirus closed the wound 24 h after scratching, whereas those infected with EGFP-RA mutant-expressing adenovirus did not (Fig. 8*B*). To exclude the possibility that RA mutant-expressing cells moved more slowly than EGFP-expressing cells, we monitored randomly migrating cells expressing either RA mutant or EGFP. There was no significant change of the migratory velocity between two groups (Sup-

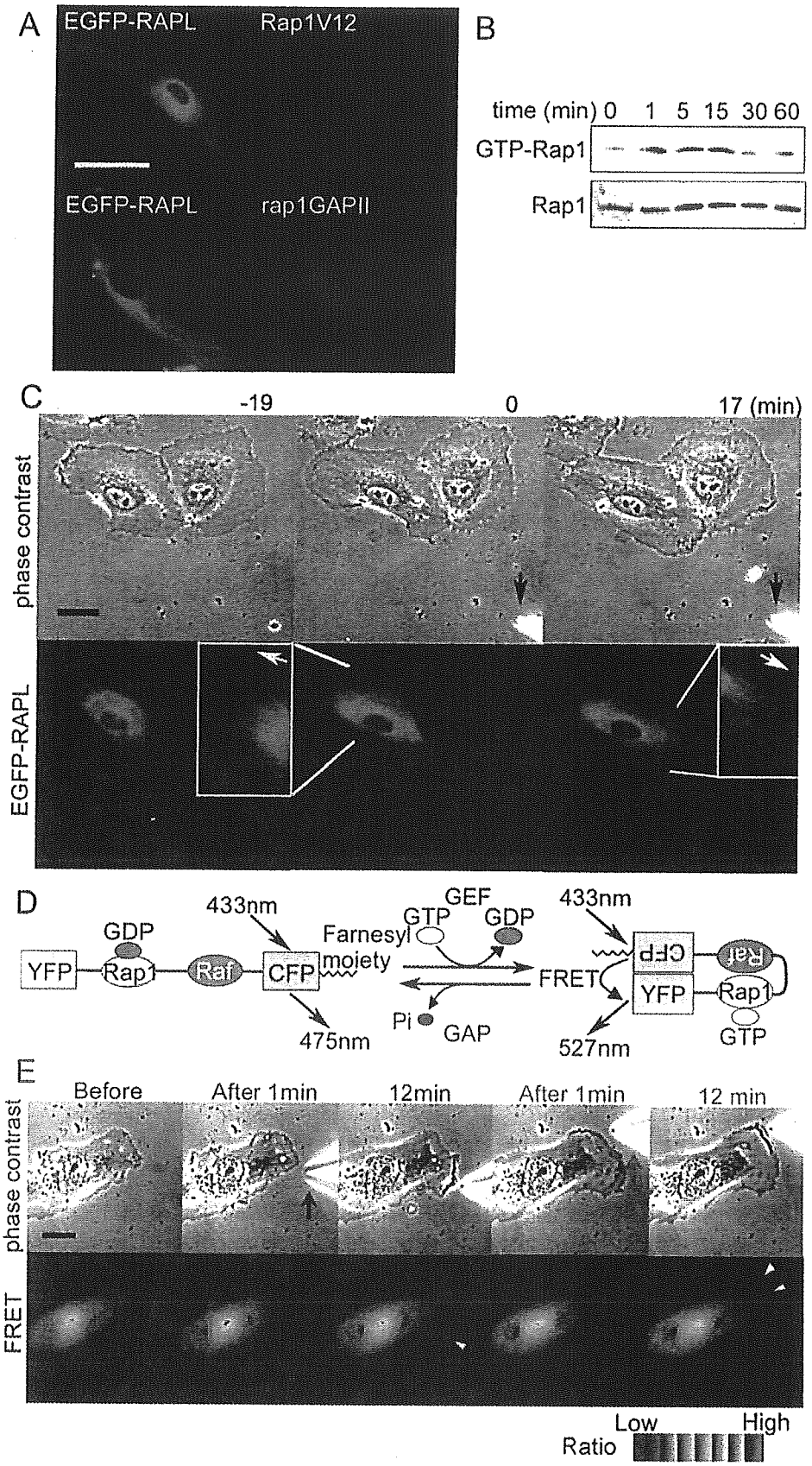

FIG. 5. **Rap1 regulates the localization of RAPL and precedes the extension of microtubules toward the leading edge of migrating cells upon chemotactic S1P stimulation.** *A*, HAECs were co-transfected with pCA-EGFP-RAPL and either pIRM21-Rap1V12 (*top*) or pIRM21-rap1GAPII (*bottom*). Note that EGFP-RAPL is dissociated from microtubules in Rap1V12-expressing cells, whereas EGFP-RAPL is associated with microtubules in rap1GAPII-expressing cells. *B*, HAECs stimulated with 1 μM S1P during the time period indicated at the *top* were lysed and analyzed by Bos's pull-down method using the GST-Rap1 binding domain of RalGDS. *C*, HAECs expressing EGFP-RAPL were time lapse-imaged before (−19 min) and after (17 min) the point (0) when 1 μM S1P was applied from a micropipette. Note that at time point 0, the cell

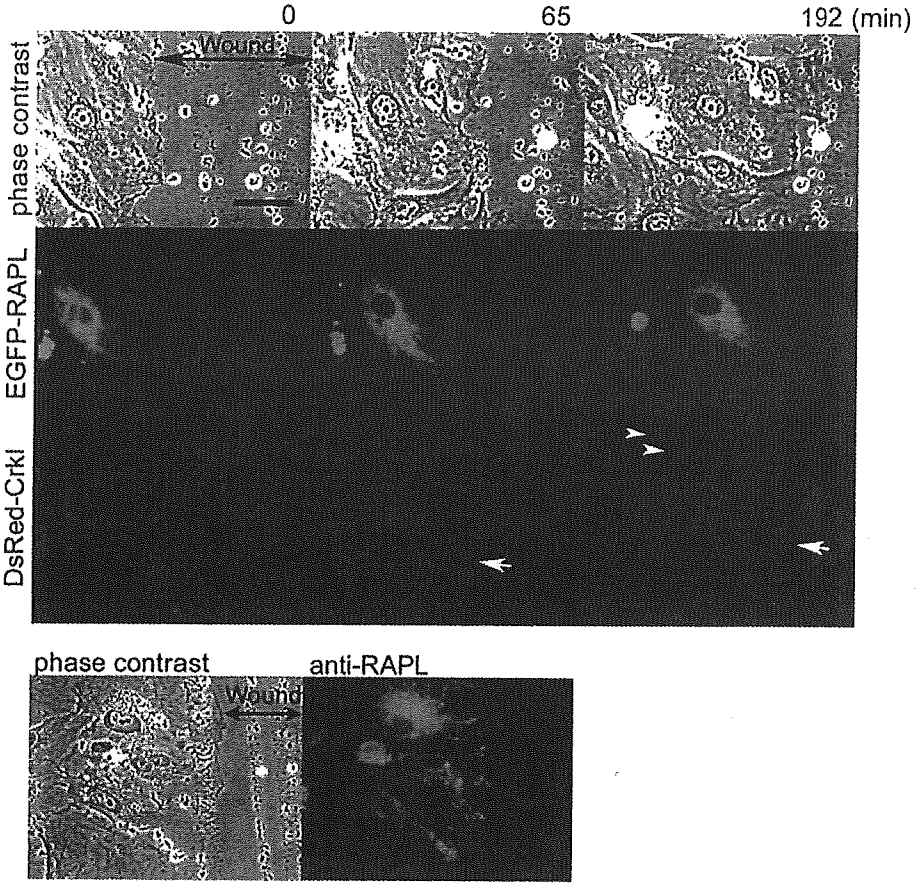

FIG. 6. **Microtubules marked by EGFP-RAPL grow toward the leading edge during wound healing.** *A*, monolayer-cultured HAECs expressing both EGFP-RAPL and DsRed-CrkI were time lapse-imaged after scratching. Phase-contrast (*top*), EGFP (*middle*), and DsRed (*bottom*) images were obtained through Olympus IX81 fluorescent microscope at the time point after scratching as indicated at the *top*. The *arrows* in the *bottom panel* indicate the nascent focal complexes at the leading edge, whereas the *arrowheads* indicate the focal adhesions in the retracting region. Note that microtubules marked by EGFP-RAPL grow toward the leading edge marked by DsRed-CrkI. *Wound*, scratched area. *Bar*, 50 μm. A series of time lapse images of phase-contrast, EGFP, and DsRed view were converted to a video (Supplemental Video 7). *B*, monolayer-cultured HAECs were immunostained with anti-RAPL 4 h after scratching. Phase contrast (*left*) and immunostaining with anti-RAPL (*right*) followed by visualization with Alexa488-conjugated secondary antibody are shown.

plemental Fig. 2*C*). These data indicated that Rap1 activation and subsequent Rap1-RAPL association is required for directional movement of endothelial cells during wound healing.

DISCUSSION

The directional migration is accompanied with microtubule growth toward the leading edge of migrating cells. The microtubule extension depends on the localization of microtubule-capturing or -attracting molecules. Microtubules cooperatively promote cell migration accompanied with cell polarization together with actin cytoskeleton (35, 36). Extracellular stimuli activating Rho family proteins, Rho, Rac, and Cdc42, via plasma membrane receptors and cell-ECM complexes determine the direction of microtubule growth (28). Therefore, the downstream effectors of Rho family proteins are proposed to function as microtubule-capturing molecules at the cell cortex. Such candidate systems include Cdc42-Par6-protein kinase Cζ-dynein and Rac/Cdc42-IQGAP-CLIP170 (35, 38). Here we demonstrate, for the first time, that Rap1-RAPL signaling contributes to determining the direction of cell migration accompanied with microtubule growth upon chemoattractant stimulation and during wound healing.

Given that RAPL was expressed in vascular endothelial cells and associated with GTP-Rap1, it is important to ask where and how RAPL is regulated by active Rap1 in living cells. To answer this question, we first examined the localization of RAPL and found that RAPL localized on microtubules from MTOC to the periphery. Previously, it has been reported that Rassf1A localizes on microtubules in a variety of cells (22) and participates in mitosis by inhibiting the binding of anaphase-promoting complex to Cdc20 (39) or by stabilizing microtubules for tumor suppression (22). Rassf members were originally isolated as tumor suppressors. Thus, Rassfs have been mainly focused on as regulators of tumor suppression. We noticed that microtubules found in HAECs transfected with pEGFP-Rassf1A and -1C were different from those found in HAECs transfected with pCA-EGFP-RAPL. Rassf1 appeared to deform and thicken microtubules, whereas RAPL seemed to localize on endogenous microtubules. Recently, Rassf1A and -1C are re-

moving toward the left top corner exhibited microtubules growing in the same direction as the cell movement. An *enlarged image* is shown in the *white box* (*bottom left*). Upon start of the S1P application, the cell turn to the micropipette tip (*black arrows*), began to move and exhibited a protrusion toward the tip, in which the microtubules extended forward along the direction of movement. An *enlarged image* is shown in the *white box* (*bottom right*). The *white arrows* indicate the moving direction. A series of phase-contrast images and EGFP images were converted into a video (Supplemental Video 3). *Bar*, 40 μm. *D*, schematic illustration of Raichu-Rap1. FRET efficiency depends on the guanine nucleotide binding. GDP-bound Raichu-Rap1 emits 475-nm fluorescence when excited at 433 nm, whereas GTP-bound Raichu-Rap1 emits 527-nm fluorescence due to FRET. *Raf*, Ras/Rap1 binding domain of Raf. *E*, HAECs expressing Raichu-Rap1 were imaged during exposure to S1P from the micropipette tip. Phase-contrast images and FRET images were obtained before and after the S1P stimulation. The time points indicated at the *top* show the first location and stimulation with S1P (*black*), the relocation of the tip, and the stimulation with S1P (*red*). Note that increased FRET reflecting Rap1 activation was observed at the edge of protrusion toward the micropipette tip. *Red* and *blue hue* indicate the increased and decreased FRET, respectively. The *arrowheads* indicate the activated Rap1 shown by the increased FRET. A series of phase-contrast images and FRET images were converted to a video (Supplemental Video 4). HAECs expressing Raichu-Rap1N17 was FRET-imaged during exposure to S1P from the micropipette tip similarly to Raichu-Rap1. Note that FRET does not occur at the ruffled membrane induced by S1P (Supplemental Video 5). Untransfected HAECs do not exhibit membrane ruffles in response to S1P-free medium (Supplemental Video 6).

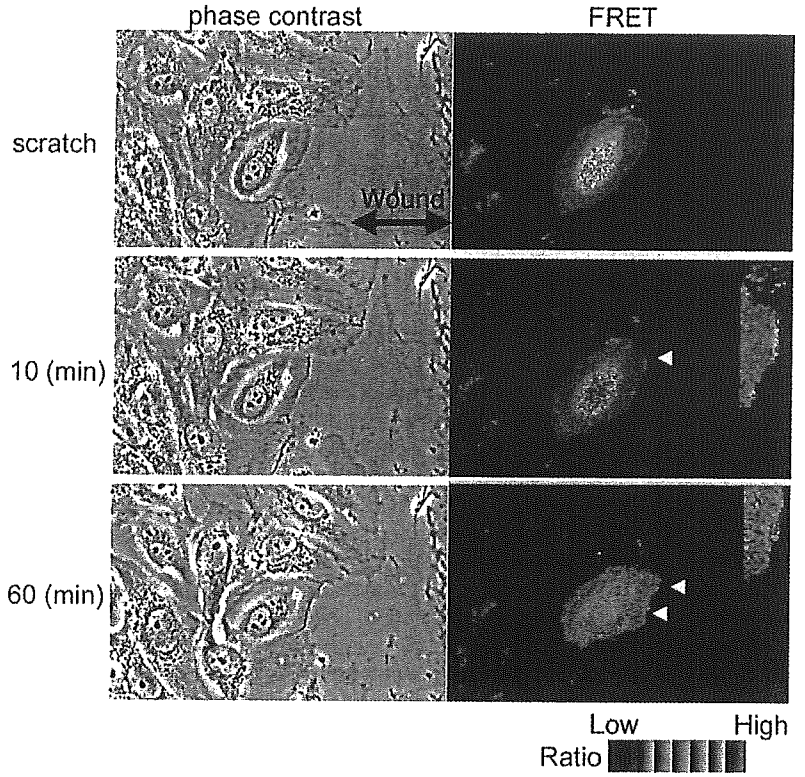

FIG. 7. **Rap1 is activated at the leading edge of the migrating cells.** HAECs cultured as a monolayer sheet transfected with pRaichu-Rap1 were scratched (*scratch*) and time lapse-imaged for phase-contrast and FRET observations. The elapsed time after scratching is indicated on the *left*. The *red hue* and *blue hue* in the FRET images indicate an increase (*high*) and a decrease (*low*) in the ratio of YFP to CFP, reflecting Rap1 activation and inactivation, respectively. The *arrowheads* indicate the activation of Rap1 at the leading edge of the cells migrating into the wound. The regions pointed out by the *arrows* are *enlarged* and shown in the *right corner* in the same *panel*. *Wound*, scratched area.

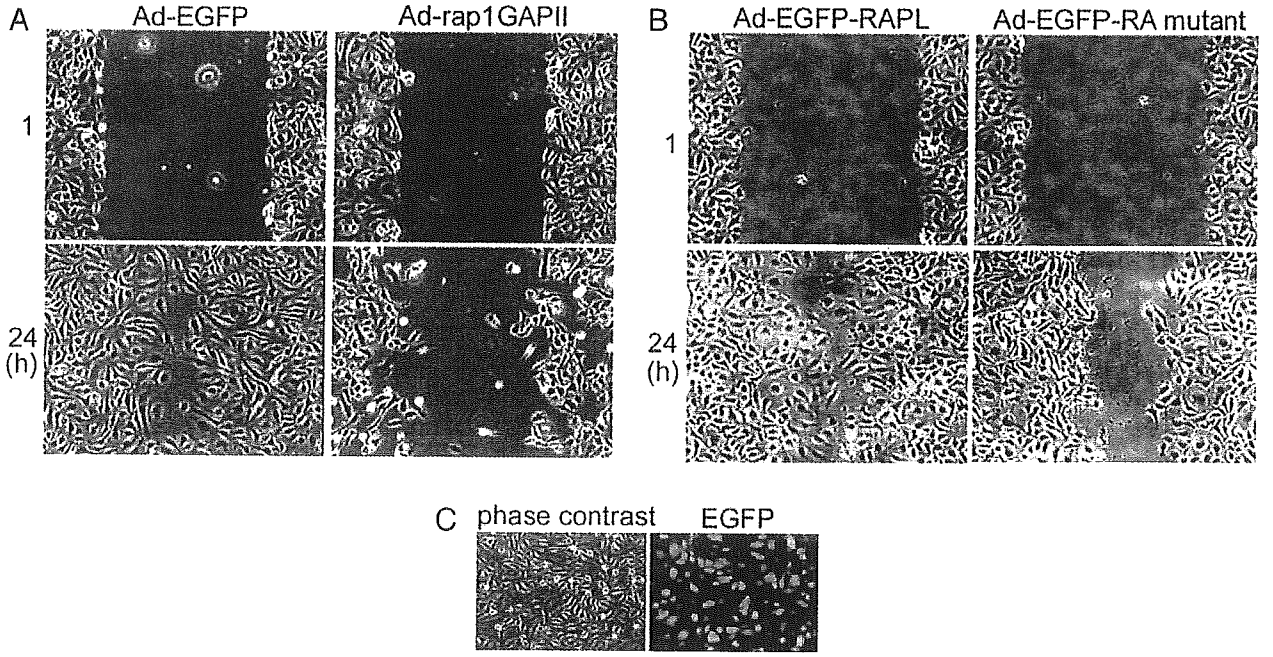

FIG. 8. **Rap1 activation and subsequent Rap1-RAPL association are required for wound healing.** *A*, HUVECs were either infected for 24 h with adenovirus expressing EGFP (Ad-EGFP) or adenovirus expressing rap1GAPII (Ad-rap1GAPII). 24 h after infection, the monolayer HUVECs were wounded by scratching. The wound healing was monitored at the time point as indicated on the *left*. Note that the cells expressing EGFP used as a control healed the wound, whereas the cells expressing rap1GAPII could not. HAECs infected with GFP-expressing adenovirus for 24 h were imaged. *B*, similarly to *A*, HUVECs were infected with either an adenovirus expressing EGFP-RAPL (Ad-EGFP-RAPL) or that expressing the EGFP-RA mutant of RAPL (Ad-EGFP-RA mutant). 24 h after scratching, cells were imaged. Note that the RAPL-expressing cells closed the wound, whereas those expressing RA mutant did not. *C*, the efficiency of infection was confirmed by the expression of EGFP in HUVECs infected with an adenovirus-expressing EGFP.

ported to suppress tumors by stabilizing microtubules and maintaining genomic stability (40). The circular fibers found in the EGFP-Rassf1-expressing cells appear to reflect the stabilized microtubules. Furthermore, although Rassf1A-transfected cells exhibited the membrane ruffling, microtubules marked by EGFP-Rassf1A did not grow or shrink at all (Fig. 2 and Supplemental Videos 1 and 2, *left*). In clear contrast, EGFP-tagged RAPL and endogenous RAPL localizes on microtubules (Figs. 2*D* and 3 and Supplemental Videos 1 and 3, *right*). RAPL dislocated from microtubules when cells were transfected with Rap1V12-expressing plasmids (Fig. 5*A*). In addition, inactivation of Rap1 and disconnection between Rap1 and RAPL perturbed the directional migration (Fig. 8). These results imply that Rap1-RAPL signal may participate in regu-

lation of microtubule growth. Further study is required to decipher the mechanism by which Rap1-RAPL-mediated signal regulates microtubule growth and/or stabilization.

Microtubules marked by EGFP-RAPL grew toward the leading edge, where DsRed-CrkI assembled as focal adhesions during wound healing. C3G is an Src homology 3 domain-binding protein of Crk and is required for stabilizing focal adhesions (7, 41). Thus, Rap1, a substrate of C3G, was likely to be activated at the assembly of focal adhesions. We used a FRET-based probe for visualizing Rap1 activation during wound healing. As expected, Rap1 was activated at the ruffled membrane where focal complexes were about to be assembled (Fig. 7). Thus, Rap1 activation at the leading edge preceded the directional migration. Rac1 activated downstream of CrkI via DOCK180 may tether microtubules through Rac1-binding protein, IQ-GAP1, and microtubule tip protein, CLIP-170 (42).

Microtubules have been suggested to target to focal adhesion, subsequently being captured and stabilized at focal adhesions (14, 15). We have not revealed the complex of Rap1-RAPL-microtubule at focal adhesions; however, Rap1 stabilizes focal adhesions, thereby indirectly contributing to the extension of microtubules. We have previously shown that Rap1 tightens the adhesion of cell-ECM complex (7) and that Rap1 is involved in maturation of focal complex to focal adhesions (24). RAPL was dislocated from the microtubules when constitutive active Rap1 was expressed (Fig. 5*A*). Katagiri *et al.* (16) reported that RAPL stabilizes the integrin-mediated cell attachment in lymphocytes stimulated with SDF-1. Accordingly, Rap1 activated at the focal adhesion may associate with RAPL, thereby stabilizing integrin-mediated focal adhesion to which microtubules target.

S1P triggers membrane ruffling, a hallmark of cell migration (26). We demonstrated that Rap1 was activated at S1P-induced membrane ruffling (Fig. 5). Membrane ruffling is the reorganization of actin by activated Rac. Rac activation downstream of Rap1 was previously reported in the Rap1-dependent secretory pathway (43). Rap1 promotes membrane extension by activating Rac via Vav2 and Tiam1 (44). Very recently, RIAM has been found to bind GTP-bound Rap1 and enhance integrin-mediated cell adhesion by regulating actin cytoskeleton (45). Thus, Rap1 appears to extend membranes by not only stabilizing integrin-mediated cell adhesion but activating Rac. Notably, microtubules marked by EGFP-RAPL grew toward locally activated Rap1 by S1P in the ruffled membrane. Although it is uncertain whether Rac activation is required for Rap1-RAPL-mediated signaling, Rac activation by S1P in parallel with or downstream of Rap1 may contribute to microtubule extension where RAPL localizes.

FRET-based probes, which can be introduced into living cells, have enabled us to monitor the spatial and temporal activation of signaling molecules: the activation of Ras superfamily members upon EGF-stimulation (4), the involvement of Crk in S1P-triggered signaling (26), and Rac activation during cell migration (37). We have previously shown that the phosphorylation of Crk was prominent at the S1P-induced membrane ruffling in vascular endothelial cells (26). Therefore, Rap1 activation by S1P in the present data is consistent with our previous data in that Crk-Rap1 signaling is triggered by S1P. During wound healing, Crk accumulated at focal adhesions and focal complexes near the leading edge. Although we could show Rap1 activation at the leading edge, it will be necessary to monitor the precise local activation of Rap1 at focal adhesions.

In conclusion, we have demonstrated that locally activated Rap1 regulates the directional cell migration accompanied by microtubule extension, presumably by dissociating RAPL from microtubules.

Acknowledgments—We thank M. Matsuda for advice; N. Yamagishi for the purified microtubules; H. Kurose and S. Hattori for the EGFP-expressing adenovirus and the rap1GAPII-expressing adenovirus, respectively; T. Kinashi for the anti-RAPL antibody; J. T. Pearson for critical reading of the manuscript; and M. Sone, M. Miyabayashi, K. Yamamoto, and N. Irisawa for technical assistance.

REFERENCES

1. Bos, J. L. (1998) *EMBO J.* **17,** 6776–6782
2. Bos, J. L., de Rooij, J., and Reedquist, K. A. (2001) *Nat. Rev. Mol. Cell. Biol.* **2,** 369–377
3. Ohba, Y., Kurokawa, K., and Matsuda, M. (2003) *EMBO J.* **22,** 859–869
4. Mochizuki, N., Yamashita, S., Kurokawa, K., Ohba, Y., Nagai, T., Miyawaki, A., and Matsuda, M. (2001) *Nature* **411,** 1065–1068
5. Reedquist, K. A., Ross, E., Koop, E. A., Wolthuis, R. M., Zwartkruis, F. J., van Kooyk, Y., Salmon, M., Buckley, C. D., and Bos, J. L. (2000) *J. Cell Biol.* **148,** 1151–1158
6. Katagiri, K., Hattori, M., Minato, N., Irie, S., Takatsu, K., and Kinashi, T. (2000) *Mol. Cell. Biol.* **20,** 1956–1969
7. Ohba, Y., Ikuta, K., Ogura, A., Matsuda, J., Mochizuki, N., Nagashima, K., Kurokawa, K., Mayer, B. J., Maki, K., Miyazaki, J., and Matsuda, M. (2001) *EMBO J.* **20,** 3333–3341
8. Kinbara, K., Goldfinger, L. E., Hansen, M., Chou, F. L., and Ginsberg, M. H. (2003) *Nat. Rev. Mol. Cell. Biol.* **4,** 767–776
9. Park, H. O., Sanson, A., and Herskowitz, I. (1999) *Genes Dev.* **13,** 1912–1917
10. Knox, A. L., and Brown, N. H. (2002) *Science* **295,** 1285–1288
11. Pollard, T. D., and Borisy, G. G. (2003) *Cell* **112,** 453–465
12. Ridley, A. J., Schwartz, M. A., Burridge, K., Firtel, R. A., Ginsberg, M. H., Borisy, G., Parsons, J. T., and Horwitz, A. R. (2003) *Science* **302,** 1704–1709
13. Small, J. V., Geiger, B., Kaverina, I., and Bershadsky, A. (2002) *Nat. Rev. Mol. Cell. Biol.* **3,** 957–964
14. Krylyshkina, O., Anderson, K. I., Kaverina, I., Upmann, I., Manstein, D. J., Small, J. V., and Toomre, D. K. (2003) *J. Cell Biol.* **161,** 853–859
15. Kaverina, I., Rottner, K., and Small, J. V. (1998) *J. Cell Biol.* **142,** 181–190
16. Katagiri, K., Maeda, A., Shimonaka, M., and Kinashi, T. (2003) *Nat. Immunol.* **4,** 741–748
17. Hesson, L., Dallol, A., Minna, J. D., Maher, E. R., and Latif, F. (2003) *Oncogene* **22,** 947–954
18. Vos, M. D., Martinez, A., Ellis, C. A., Vallecorsa, T., and Clark, G. J. (2003) *J. Biol. Chem.* **278,** 21938–21943
19. Vos, M. D., Ellis, C. A., Bell, A., Birrer, M. J., and Clark, G. J. (2000) *J. Biol. Chem.* **275,** 35669–35672
20. Vos, M. D., Ellis, C. A., Elam, C., Ulku, A. S., Taylor, B. J., and Clark, G. J. (2003) *J. Biol. Chem.* **278,** 28045–28051
21. Shivakumar, L., Minna, J., Sakamaki, T., Pestell, R., and White, M. A. (2002) *Mol. Cell. Biol.* **22,** 4309–4318
22. Liu, L., Tommasi, S., Lee, D. H., Dammann, R., and Pfeifer, G. P. (2003) *Oncogene* **22,** 8125–8136
23. Lee, M. J., Thangada, S., Paik, J. H., Sapkota, G. P., Ancellin, N., Chae, S. S., Wu, M., Morales-Ruiz, M., Sessa, W. C., Alessi, D. R., and Hla, T. (2001) *Mol. Cell* **8,** 693–704
24. Nagashima, K., Endo, A., Ogita, H., Kawana, A., Yamagishi, A., Kitabatake, A., Matsuda, M., and Mochizuki, N. (2002) *Mol. Biol. Cell* **13,** 4231–4242
25. Franke, B., Akkerman, J. W., and Bos, J. L. (1997) *EMBO J.* **16,** 252–259
26. Endo, A., Nagashima, K., Kurose, H., Mochizuki, S., Matsuda, M., and Mochizuki, N. (2002) *J. Biol. Chem.* **277,** 23747–23754
27. Kogata, N., Masuda, M., Kamioka, Y., Yamagishi, A., Endo, A., Okada, M., and Mochizuki, N. (2003) *Mol. Biol. Cell* **14,** 3553–3564
28. Wittmann, T., and Waterman-Storer, C. M. (2001) *J. Cell Sci.* **114,** 3795–3803
29. Schaller, M. D., and Parsons, J. T. (1995) *Mol. Cell. Biol.* **15,** 2635–2645
30. Vuori, K., Hirai, H., Aizawa, S., and Ruoslahti, E. (1996) *Mol. Cell. Biol.* **16,** 2606–2613
31. Webb, D. J., Parsons, J. T., and Horwitz, A. F. (2002) *Nat. Cell Biol.* **4,** E97–E100
32. Kiyokawa, E., Mochizuki, N., Kurata, T., and Matsuda, M. (1997) *Crit. Rev. Oncog.* **8,** 329–342
33. Mochizuki, N., Ohba, Y., Kiyokawa, E., Kurata, T., Murakami, T., Ozaki, T., Kitabatake, A., Nagashima, K., and Matsuda, M. (1999) *Nature* **400,** 891–894
34. van den Berghe, N., Cool, R. H., Horn, G., and Wittinghofer, A. (1997) *Oncogene* **15,** 845–850
35. Rodriguez, O. C., Schaefer, A. W., Mandato, C. A., Forscher, P., Bement, W. M., and Waterman-Storer, C. M. (2003) *Nat. Cell Biol.* **5,** 599–609
36. Goode, B. L., Drubin, D. G., and Barnes, G. (2000) *Curr. Opin. Cell Biol.* **12,** 63–71
37. Itoh, R. E., Kurokawa, K., Ohba, Y., Yoshizaki, H., Mochizuki, N., and Matsuda, M. (2002) *Mol. Cell. Biol.* **22,** 6582–6591
38. Gundersen, G. G. (2002) *Nat. Rev. Mol. Cell. Biol.* **3,** 296–304
39. Song, M. S., Song, S. J., Ayad, N. G., Chang, J. S., Lee, J. H., Hong, H. K., Lee, H., Choi, N., Kim, J., Kim, H., Kim, J. W., Choi, E. J., Kirschner, M. W., and Lim, D. S. (2004) *Nat. Cell Biol.* **6,** 129–137
40. Vos, M. D., Martinez, A., Elam, C., Dallol, A., Taylor, B. J., Latif, F., and Clark, G. J. (2004) *Cancer Res.* **64,** 4244–4250
41. Caron, E., Self, A. J., and Hall, A. (2000) *Curr. Biol.* **10,** 974–978
42. Fukata, M., Watanabe, T., Noritake, J., Nakagawa, M., Yamaga, M., Kuroda, S., Matsuura, Y., Iwamatsu, A., Perez, F., and Kaibuchi, K. (2002) *Cell* **109,** 873–885
43. Maillet, M., Robert, S. J., Cacquevel, M., Gastineau, M., Vivien, D., Bertoglio, J., Zugaza, J. L., Fischmeister, R., and Lezoualc'h, F. (2003) *Nat. Cell Biol.* **5,** 633–639
44. Arthur, W. T., Quilliam, L. A., and Cooper, J. A. (2004) *J. Cell Biol.* **167,** 111–122
45. Lafuente, E. M., van Puijenbroek, A. A., Krause, M., Carman, C. V., Freeman, G. J., Berezovskaya, A., Constantine, E., Springer, T. A., Gertler, F. B., and Boussiotis, V. A. (2004) *Dev. Cell* **7,** 585–595

MOLECULAR AND CELLULAR BIOLOGY, Jan. 2005, p. 136–146 Vol. 25, No. 1
0270-7306/05/$08.00+0 doi:10.1128/MCB.25.1.136–146.2005

Cyclic AMP Potentiates Vascular Endothelial Cadherin-Mediated Cell-Cell Contact To Enhance Endothelial Barrier Function through an Epac-Rap1 Signaling Pathway

Shigetomo Fukuhara,[1] Atsuko Sakurai,[1] Hideto Sano,[2] Akiko Yamagishi,[1] Satoshi Somekawa,[1,3] Nobuyuki Takakura,[2] Yoshihiko Saito,[3] Kenji Kangawa,[4] and Naoki Mochizuki[1]*

Department of Structural Analysis[1] and Department of Biochemistry,[4] National Cardiovascular Center Research Institute, Osaka, Department of Stem Cell Biology, Cancer Research Institute, Kanazawa University, Kanazawa,[2] and First Department of Internal Medicine, Nara Medical University, Nara,[3] Japan

Received 2 August 2004/Returned for modification 2 September 2004/Accepted 28 September 2004

Cyclic AMP (cAMP) is a well-known intracellular signaling molecule improving barrier function in vascular endothelial cells. Here, we delineate a novel cAMP-triggered signal that regulates the barrier function. We found that cAMP-elevating reagents, prostacyclin and forskolin, decreased cell permeability and enhanced vascular endothelial (VE) cadherin-dependent cell adhesion. Although the decreased permeability and the increased VE-cadherin-mediated adhesion by prostacyclin and forskolin were insensitive to a specific inhibitor for cAMP-dependent protein kinase, these effects were mimicked by 8-(4-chlorophenylthio)-2′-*O*-methyladenosine-3′, 5′-cyclic monophosphate, a specific activator for Epac, which is a novel cAMP-dependent guanine nucleotide exchange factor for Rap1. Thus, we investigated the effect of Rap1 on permeability and the VE-cadherin-mediated cell adhesion by expressing either constitutive active Rap1 or Rap1GAPII. Activation of Rap1 resulted in a decrease in permeability and enhancement of VE-cadherin-dependent cell adhesion, whereas inactivation of Rap1 had the counter effect. Furthermore, prostacyclin and forskolin induced cortical actin rearrangement in a Rap1-dependent manner. In conclusion, cAMP-Epac-Rap1 signaling promotes decreased cell permeability by enhancing VE-cadherin-mediated adhesion lined by the rearranged cortical actin.

Endothelial cells lining blood vessels regulate endothelial barrier function, which restricts the passage of plasma proteins and circulating cells across the endothelial cells. Endothelial barrier dysfunction results in an increase in vascular permeability, thereby causing edema or inflammatory or metastatic cell infiltration. Inflammatory mediators such as thrombin and histamine induce intercellular gap formation, leading to an increase in endothelial permeability (1, 4). In contrast, angiopoietin 1 and sphingosine-1-phosphate (S1P) stabilize endothelial barrier integrity (17, 18). In addition, cyclic AMP (cAMP), a second messenger downstream of Gs-coupled receptor, improves endothelial cell barrier function (32, 39, 43). Consistently, cAMP-elevating G protein-coupled receptor (GPCR) agonists, adrenomedullin (AM), prostacyclin (PGI2), prostaglandin E2 (PGE2), and β-adrenergic agonists reduce endothelial hyperpermeability induced by inflammatory stimuli (15, 19, 25).

The endothelial cell barrier is structurally organized by adherens junctions (AJ) and tight junctions. Vascular endothelial (VE) cells express both VE-cadherin (also known as cadherin-5 and CD144) and neural (N)-cadherin (9, 33). VE-cadherin constitutes AJ, whereas N-cadherin formed the cell-cell contacts between endothelial cells and endothelial cell-supporting pericytes. VE-cadherin mediates calcium-dependent, homophilic intercellular adhesion. Its short cytoplasmic tail binds to three armadillo family proteins, β-, γ-, and p120-catenins. β- and γ-catenins associated with α-catenin link the VE-cadherin complex to the actin cytoskeleton and, therefore, strengthen the AJ adhesiveness (9).

Endothelial AJ are dynamic structures, and their adhesive property is finely regulated by several different mechanisms. Tyrosine phosphorylation of VE-cadherin, β-catenin, and p120-catenin correlates with weakened endothelial cell-cell adhesion. VE growth factors and inflammatory mediators such as histamine and thrombin induce tyrosine phosphorylation of AJ components, resulting in the weakened cell-cell contacts and increased endothelial cell permeability (1, 14, 40). In clear contrast, angiopoietin 1, which stabilizes cell-cell contacts, induces dephosphorylation of endothelial cell adhesion molecules, VE-cadherin, and platelet endothelial cell adhesion molecule 1 (17). It has been also reported that S1P induces AJ formation and enhances barrier function through a Rac-dependent cortical actin rearrangement (18). cAMP-dependent protein kinase A (PKA) is suggested to be crucial for cAMP-triggered stabilization of cell-cell contacts and for barrier integrity of endothelial cells (43). However, it has not been clear whether PKA-independent signaling is involved in the regulation of endothelial barrier function.

Rap1, belonging to Ras family GTPase, is involved in the formation and stabilization of AJ in *Drosophila melanogaster* (23). Rap1 becomes the GTP-bound active form by guanine

* Corresponding author. Mailing address: Department of Structural Analysis, National Cardiovascular Center Research Institute, 5-7-1 Fujishirodai, Suita, Osaka 565-8565, Japan. Phone: 81-6-6833-5012, ext. 2508. Fax: 81-6-6835-5461. E-mail: nmochizu@ri.ncvc.go.jp.

nucleotide exchange factor (GEF) and the GDP-bound inactive form by GTPase-activating proteins (GAP), respectively. GEFs for Rap1 include C3G, CalDAG-GEFs, Epacs, and DOCK4 (reviewed in reference 6). DOCK4, which is disrupted in various types of human cancers, regulates the formation of AJ (41). Very recent reports also revealed that Rap1 activity is required for the formation of E-cadherin-based cell-cell contacts (20, 36). These findings prompted us to investigate how Rap1 is activated to stabilize cell-cell contacts and to examine the physiological consequence of stabilized cell-cell contacts by Rap1.

In the present study, we investigated the mechanism by which cAMP-elevating GPCR agonists potentiate endothelial barrier function and restrict cell permeability. We found that increased cAMP triggers Epac-Rap1 signaling to reduce permeability independently of PKA by augmentation of VE-cadherin-mediated cell-cell adhesion.

MATERIALS AND METHODS

Reagents and antibodies. Human recombinant AM was kindly provided by Shionogi & Co. Ltd (31). Materials were purchased as follows: isoproterenol (Iso), PGE2, PGI2, thrombin, forskolin (FSK), and 3-isobutyl-1-methylxanthine (IBMX) from Wako Pure Chemical Industries; dibutyryl-cAMP (dbcAMP) from Sigma-Aldrich; H89 from Seikagaku Corporation; 8-(4-chlorophenylthio)-2′-*O*-methyladenosine-3′,5′-cyclic monophosphate (8-CPT-2′-O-Me-cAMP) from Tocris; fluorescein isothiocyanate (FITC)-labeled dextran (molecular weight, 42,000) and purified human immunoglobulin G (IgG) Fc protein from ICN Biologicals; vascular endothelial growth factor (VEGF) from R & D Systems. Anti-Rap1GAPII antibody was developed by immunization of glutathione *S*-transferase (GST)-tagged Rap1GAPII (amino acids 411 to 694 of Rap1GAPII). Other antibodies used here were purchased as follows: anti-VE-cadherin from Chemicon International and Transduction Laboratories; anti-β-catenin from Transduction Laboratories; anti-CREB and anti-phospho-CREB (Ser133) from Cell Signaling Technology; anti-Rap1 from Santa Cruz Biotechnology; anti-cortactin from Upstate Biotechnology, Inc.; rhodamine-phalloidin and Alexa 488-labeled goat anti-mouse IgG from Molecular Probes; horseradish peroxidase-coupled goat anti-mouse and goat anti-rabbit IgG from Amersham Biosciences.

Cell culture and transfection. Human umbilical vein endothelial cells (HUVECs) and human arterial endothelial cells (HAECs) were purchased from Kurabo (Kurashiki, Japan). The cells were maintained in HuMedia-EG2 with a growth additive set as described previously (12) and used for experiments before passages 7 and 10, respectively. HEK293, 293T, and HeLa cells were maintained in Dulbecco's modified Eagle's medium (DMEM; Nissui, Tokyo, Japan) supplemented with 10% fetal bovine serum and antibiotics (100 μg of streptomycin/ml and 100 U of penicillin/ml). HUVECs and 293T cells were transfected by using Lipofectamine Plus reagent (Invitrogen) and by the calcium-phosphate precipitation technique, respectively.

Plasmids and adenovirus. pcDNA-VE-cad-Ect-Fc-His is a modified vector of pcDNA3.1-Fc-PECAM-1 (a kind gift from W. A. Muller, Cornell University) for producing the secreted form of the extracellular domain of VE-cadherin fused with Fc followed by a six-His tag. A DNA fragment encoding human Epac lacking the cAMP binding domain (amino acids 324 to 881) was amplified by PCR with pMT2SM-HA-Epac (a kind gift from J. L. Bos, Utrecht University, Utrecht, The Netherlands) as a template and ligated into the pCXN2 vector (12). pCXN2-FLAG-Rap1V12-IRES-EGFP expressed both FLAG-tagged Rap1V12 and internal ribosomal entry site (IRES)-driven enhanced green fluorescent protein (EGFP), and pCXN2-Rap1GAPII-IRES-EGFP expressed both FLAG-tagged Rap1GAPII and IRES-driven EGFP. pGL3 control vector was purchased from Promega Corp. Recombinant adenoviruses encoding Rap1GAPII (Ad-RapGAP) and LacZ (Ad-LacZ) were obtained from S. Hattori (The Institute of Medical Science, University of Tokyo) and M. Matsuda (Research Institute for Microbial Disease, Osaka University, Osaka, Japan), respectively. Adenoviruses expressing FLAG-tagged Rap1V12 and IRES-driven EGFP (Ad-Flag-Rap1V12-IRES-EGFP) were produced by using the Adeno-X system according to the manufacturer's protocol (Clontech). Endothelial cells were infected with adenoviruses at the appropriate multiplicities of infection (MOI) as described in the figure legends.

Permeability assay. Permeability across the endothelial cell monolayer was measured by using type I collagen-coated transwell units (6.5-mm diameter, 3.0-μm-pore-size polycarbonate filter; Corning Costar Corporation). HUVECs plated at 10^5 cells in each well were cultured for 3 to 4 days before experiments. After serum starvation in medium 199 containing 1% bovine serum albumin (BSA) for 1 h, the cells were treated with the agonists or drugs, as indicated in the figure legends, for 30 min. Permeability was measured by adding 1 mg of FITC-labeled dextran (molecular weight, 42,000)/ml together with or without 2 U of thrombin/ml to the upper chamber. After incubation for 30 min, 50 μl of sample from the lower compartment was diluted with 300 μl of phosphate-buffered saline (PBS) and measured for fluorescence at 520 nm when excited at 492 nm with a spectrophotometer F-4500 (Hitachi). HUVECs infected with adenovirus for 24 h after becoming confluent and kept for another 24 h in replaced medium were subjected to a cell permeability assay.

Immunocytochemistry. Monolayer-cultured HUVECs grown on a 35-mm-diameter glass base dish (Asahi Techno Glass) were starved in medium 199 containing 0.5% BSA for 3 h and subsequently incubated with the stimulants indicated in the figure legends for 30 min. After stimulation, the cells were fixed in PBS containing 2% formaldehyde for 30 min at 4°C, washed with PBS, and permeabilized with 0.05% Triton X-100 for 30 min at 4°C. Cells were blocked with PBS containing 4% BSA for 1 h at room temperature (RT) and stained with rhodamine-phalloidin for 20 min, anti-VE-cadherin for 60 min, and anticortactin for 60 min at RT. Protein reacting with antibody was visualized with Alexa 488-labeled goat anti-mouse IgG. Images were recorded with a confocal microscope (BX50WI, Fluoview; Olympus) with a water immersion objective lens (LUMPlanF1 100X1.00W).

VE-cadherin translocation assay and Western blot analysis. HUVECs plated in six-well plates were serum starved in medium 199 containing 1% BSA overnight. The cells were stimulated with PGI2 and FSK for the indicated time and fractionated with cytoskeleton-stabilizing buffer (10 mM HEPES [pH 7.4], 250 mM sucrose, 150 mM KCl, 1 mM EGTA, 3 mM $MgCl_2$, 1× protease inhibitor cocktail [Roche Diagnostics], 1 mM Na_3VO_4, 0.5% Triton X-100) by centrifugation at 15,000 × *g* for 15 min. The Triton X-100-insoluble fraction was subjected to sodium dodecyl sulfate-polyacrylamide gel electrophoresis (SDS-PAGE) followed by transfer to Immobilon-P (Amersham Biosciences) and immunoblotting with the indicated antibodies. Immunocomplexes were visualized by enhanced chemiluminescence detection (Amersham Biosciences) with species-matched peroxidase-conjugated secondary antibodies.

Purification of recombinant VE-cadherin ectodomain-Fc chimeric protein. 293T cells transfected with pcDNA-VE-cad-Ect-Fc-His were cultured in DMEM supplemented with 10% fetal calf serum for 24 h and subsequently kept in replaced medium (DMEM-F21 containing 1% fetal calf serum) for 7 days. VE-cadherin-Fc (VEC-Fc) protein secreted into the medium was collected every 2 days and centrifuged to remove floating cells and debris. VEC-Fc was collected on ProBond resin (Invitrogen) by gentle agitation overnight at 4°C. VEC-Fc protein bound to the beads was eluted with 500 mM imidazole, concentrated with Amicon Centriplus 30 (Millipore), and buffer exchanged into PBS containing 2 mM $CaCl_2$ and 2 mM $MgCl_2$ (PBS-Ca/Mg) by dialysis.

Cell adhesion assay. Twenty-four-well tissue culture plates were coated with 10 μg of VEC-Fc or Fc protein/ml in PBS-Ca/Mg at 4°C overnight. After washing with PBS-Ca/Mg, the plates were blocked with 1% heat-inactivated BSA in PBS (heat inactivated at 85°C for 12 min) for 1 h at RT. To examine cell adhesion to the VEC-Fc- or Fc-coated dish, cells were suspended in 0.5% BSA-containing medium 199 and incubated for 30 min at 37°C. Cells (1.5×10^5) were plated on each VEC-Fc- or Fc-coated well in the presence or absence of agonists, drugs, and 5 mM EGTA and adhered to the dish at 37°C for the indicated time. To analyze cell adhesion to a collagen-covered surface, cells were plated onto a collagen-coated six-well plate (Iwaki) and adhered to the dish in the presence or absence of 5 mM EGTA. After washing with PBS-Ca/Mg four times to remove nonadherent cells, adherent cells and input cells were quantified by measuring endogenous alkaline phosphatase activity as described elsewhere (35). Briefly, the cells were lysed in a buffer containing 100 mM Tris-citrate (pH 6.5) and 0.25% Triton X-100, and alkaline phosphate activity in the lysate was measured by using the AttoPhos AP fluorescent substrate system (Promega Corp.). To examine the effects of Rap1V12, EpacΔcAMP, and Rap1GAPII, HUVECs were transfected with plasmids encoding either Rap1V12, EpacΔcAMP, or Rap1GAPII together with the luciferase reporter construct (pGL3 control vector). The adhesion of cells expressing Rap1V12, EpacΔcAMP, or Rap1GAPII to the VEC-Fc-coated dish was normalized by measuring the luciferase activity of the cells and input cells (16).

Detection of GTP-bound form of Rap1. Rap1 activity was assessed by a modified Bos's method as described previously (34). Briefly, HUVECs starved in medium 199 containing 1% BSA overnight were stimulated with the indicated

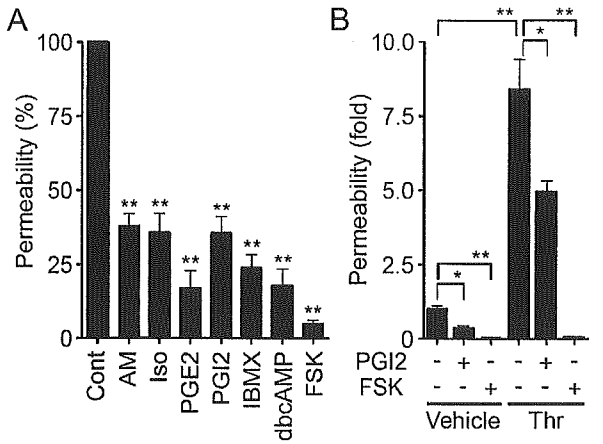

FIG. 1. cAMP enhances barrier function of monolayer VE cells. (A) Vascular permeability, reflecting barrier function, was analyzed by measuring the fluorescence of FITC-labeled dextran across the monolayer-cultured HUVECs as described in Materials and Methods. HUVECs grown on transwell filters were incubated with control (Cont), 0.1 μM AM, 200 μM Iso, 200-ng/ml PGE2, 10-μg/ml PGI2, 1 mM IBMX, 1 mM dbcAMP, and 10 μM FSK for 30 min. Average permeability ± standard deviation is expressed as a percentage compared to the control. (B) The effects of PGI2 and FSK on vascular permeability were quantified in the presence (+) or absence (−) (Vehicle) of 2 U of thrombin (Thr)/ml. Average permeability ± standard deviation is expressed as the increase relative to that observed in unstimulated HUVECs in the vehicle. Data shown are the results from at least three independent experiments. Significant differences from the control (A) or between two groups (B) determined by Student's *t* test are indicated by a single asterisk ($P < 0.05$) or double asterisks ($P < 0.01$).

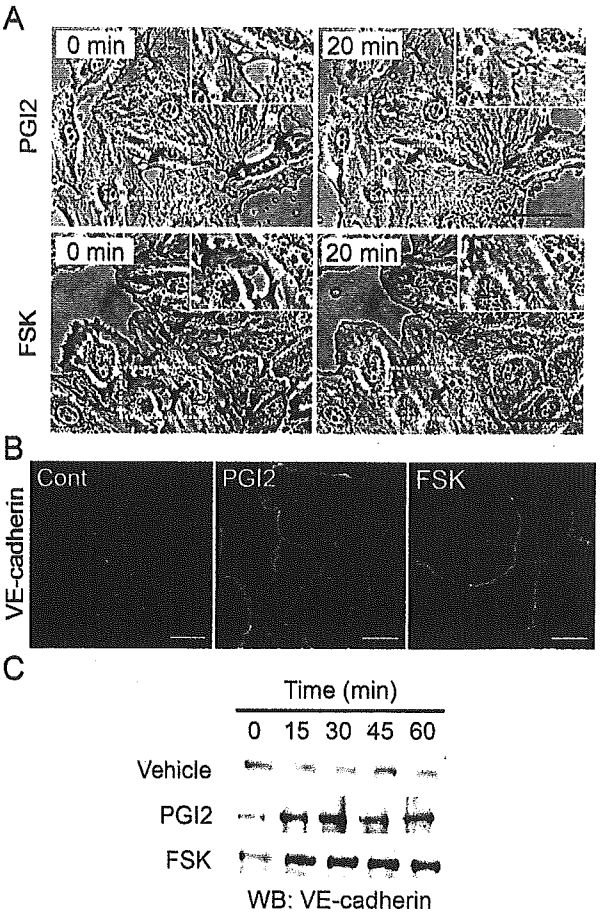

FIG. 2. cAMP induces AJ formation. (A) HUVECs cultured on a glass base dish were stimulated with 10 μg of PGI2/ml (upper panels) or with 10 μM FSK (lower panels) for 20 min and shown as phase-contrast images. Left and right panels show the cells before and after stimulation, respectively. The arrows indicate the sites of cell-cell contacts induced by PGI2 and FSK. The area boxed by the white broken line is enlarged in the right top of the panels. Bars, 50 μm. (B) Subconfluent HUVECs stimulated with vehicle (Cont), 10-μg/ml PGI2, and 10 μM FSK for 45 min were fixed, stained with anti-VE-cadherin antibody, and visualized with Alexa 488-conjugated secondary antibody through a confocal microscope (BX50WI; Olympus). Note that VE-cadherin (green) was accumulated at the cell-cell contact upon PGI2 and FSK stimulation. Bars, 50 μm. (C) Translocation of VE-cadherin was assessed by Triton X-100 solubility. HUVECs were stimulated with vehicle (top), 10-μg/ml PGI2 (middle), and 10 μM FSK (bottom) for the time indicated at the top and fractionated with cytoskeleton-stabilizing buffer as described in Materials and Methods. The Triton X-100-insoluble fraction was subjected to SDS-PAGE followed by Western blot analysis (WB) with anti-VE-cadherin.

agonists and drugs and lysed at 4°C in a pull-down lysis buffer (20 mM Tris-HCl [pH 7.5], 100 mM NaCl, 10 mM $MgCl_2$, 1% Triton X-100, 1 mM EGTA, 1 mM dithiothreitol, 1 mM Na_3VO_4, 1× protease inhibitor cocktail). GTP-bound Rap1 was collected on the GST-Rap1 binding domain of RalGDS precoupled to glutathione-Sepharose beads and subjected to SDS-PAGE followed by immunoblotting with anti-Rap1.

In vivo permeability assay. In vivo permeability was quantified by a modified Miles assay as described previously (29). In brief, ICR mice (Japan SLC, Inc.) shaved 3 days before experiments were lightly anesthetized and intravenously injected with 150 μl of 1% Evans blue dye solution (in saline) passed through a 0.22-μm-pore-size filter. Fifteen minutes later, 20 μl of PBS, VEGF (50 μg/ml), and/or 8-CPT-2′-O-Me-cAMP (1 mM) were applied by intradermal injections with a 30-gauge needle. The sites of intradermal injection were photographed 60 min after the injection, carefully dissected, and weighed. To quantify the vascular permeability, extravasated blue dye was eluted from the dissected skin with formamide at 56°C, and optical density was measured by spectrophotometry at 620 nm.

RESULTS

cAMP enhances the barrier property of monolayer-cultured endothelial cell. To evaluate the barrier function, we examined the permeability of FITC-labeled dextran across monolayer HUVECs. Expectedly, AM, Iso, PGE2, and PGI2 reduced basal endothelial permeability in HUVECs (Fig. 1A). PGI2 also reduced thrombin-induced vascular permeability (Fig. 1B). Other cAMP-elevating bio-ligands similarly reduced thrombin-induced permeability (data not shown). The bio-ligands for cAMP-elevating GPCR that we used in this study indeed increased cAMP in HUVECs (data not shown). Furthermore, IBMX (an inhibitor for phosphodiesterase), dbcAMP (a membrane-permeable cAMP analogue), and FSK (an adenylyl cyclase activator) resulted in a reduction of both basal and thrombin-induced endothelial permeability (Fig. 1; data not shown).

cAMP potentiates formation of AJ. Endothelial barrier function is largely dependent upon endothelial cell junctions. To investigate how cAMP affects AJ formation, we examined AJ organization by immunostaining with anti-VE-cadherin before and after stimulation. When subconfluent HUVECs with intercellular gaps were stimulated with PGI2 or FSK, the cells extended the plasma membrane and established cell-cell contacts with neighboring cells (Fig. 2A). Similar results were